Journal Pre-proofs

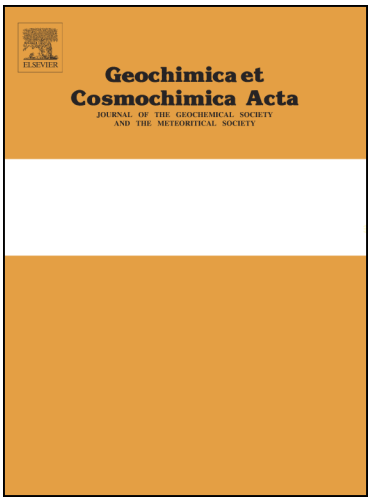

Diversity among fossil micrometeorites in the late Devonian

Krämer Ruggiu Lisa, Villeneuve Johan, Da Silva Anne-Christine, Debaille Vinciane, Decrée Sophie, Lutz Hecht, Felix E.D. Kaufmann, Goderis Steven

PII: S0016-7037(25)00379-5
DOI: https://doi.org/10.1016/j.gca.2025.07.016
Reference: GCA 13929

To appear in: *Geochimica et Cosmochimica Acta*

Received Date: 15 January 2025
Accepted Date: 19 July 2025

Please cite this article as: Lisa, K.R., Johan, V., Anne-Christine, D.S., Vinciane, D., Sophie, D., Hecht, L., Kaufmann, F.E.D., Steven, G., Diversity among fossil micrometeorites in the late Devonian, *Geochimica et Cosmochimica Acta* (2025), doi: https://doi.org/10.1016/j.gca.2025.07.016

Diversity among fossil micrometeorites in the late Devonian.

Krämer Ruggiu Lisa[1], Villeneuve Johan[2], Da Silva Anne-Christine[3], Debaille Vinciane[4], Decrée Sophie[5], Lutz Hecht[6], Felix E. D. Kaufmann[6], Goderis Steven[1]

[1] Archaeology, Environmental Changes & Geo-Chemistry, Vrije Universiteit Brussel, Brussels, Belgium (lisa.kramer.ruggiu@vub.be).

[2] CRPG, CNRS, Université de Lorraine, UMR 7358, Vandoeuvre-lès-Nancy, 54501, France.

[3] SediCClim Laboratory, Geology department, Liège University, Liège, Belgium.

[4] Laboratoire G-Time, Université Libre de Bruxelles, Brussels, Belgium.

[5] Institute of Natural Sciences, Geological Survey of Belgium, Brussels, Belgium.

[6] Museum für Naturkunde, Leibniz-Institut für Evolutions- und Biodiversitätsforschung, Invalidenstrasse 43, Berlin 10115, Germany

Abstract

A total of 1222 Micrometeorites (MMs) from the late Devonian period were extracted from 26 kg of carbonates host rock fragments from the Chanxhe section in Belgium, from the Latest Famennian around 360 Myr, through magnetic separation and optical picking following dissolution with mild HCl, making it one of the largest fossil MMs collection, the largest from the late Devonian. The collection shows a wide diversity of texture, comparable to modern day collection but with different distribution. The majority of the MMs were I-type (90 %), with G-type particles constituting 6 % and S-type particles at 1 %. Some of the S-types spherules are amongst the first silicate-type spherules, and amongst the most well-preserved in terms of texture and composition, to be described in fossil MMs collections. Additionally, intermediate type G/I representing < 1 % of the sample are introduced for future fossil MMs classification.

Distinguishing extraterrestrial (ET) MMs from terrestrial spherules is challenging due to weathering effects that modify both texture and composition during long residency time on Earth. The $Na_2O + K_2O$ versus Fe/Si ratio plot is used for distinguishing ET from terrestrial spherules. Using textural and compositional data in combination creates a reliable ET spherule identification.

I-type spherules show significant terrestrial alteration with notable loss of Ni and Cr, also observed in S-type spherules, with their silicate phases recrystallized in palagonite. G-type spherules display a mix of characteristics from I-type and S-type MMs. The study also highlights the presence of smaller spherules (<125 µm) compared to modern micrometeorites (210–330 µm), attributed to the predominance of I- and G-type spherules and long-term dissolution effects.

Despite some alteration for some spherules, due diagenesis of the sedimentary host rocks, the collection shows extremely well-preserved spherules, with even some oxygen isotopes signature being preserved. Indeed, triple oxygen isotope analysis reveals that 5.8 % of the particles are related to ordinary chondrites (OC) and 33 % to carbonaceous chondrites (CCs), yielding a CC/OC ratio of approximately 5.6, with comparable distribution for all major types. Also, 9 % of I- and G/I-types are OC-related. Most I-type spherules likely originate from CM, CR, or H chondrites, with some possibly from iron meteorites. The findings suggest that the source materials of the ET flux have remained relatively consistent over the past 360 Myr, providing insights into historical Solar System events and Earth's environmental changes and extends the study of ET flux to Earth to CC compared to meteorites. In addition, combined with chemical and isotopic proxies and chrome spinel, the fossil MMs could assess the complete flux of cosmic dust to Earth. Finally, the use of fossil MMs could represent potential proxies for paleo-atmospheric oxygen levels and CO_2 contents.

I. Introduction

Since the Solar System's formation, extraterrestrial (ET) material has continuously accreted to the Earth, composing a flux ranging from kilometer-scale and meter-sized meteorites to cosmic dust (Rubin and Grossman, 2010). The majority of the ET flux to Earth is originating from the main asteroid belt, between Mars and Jupiter (Genge et al., 2008; Janches et al., 2001; Love and Brownlee, 1991), while a fraction also samples comets (Noguchi et al., 2015). The inner main asteroid belt has evolved through time due to dynamical interaction of large bodies and impacts events (Morbidelli et al., 2015; Bottke et al., 2015), releasing dust in the solar system.

The modern-day ET input is estimated to be ~40,000 ± 20,000 metric tons every year (Love and Brownlee, 1993), mostly composed of small-sized particles (Schmitz et al., 2019b). Indeed, the flux of ET material arriving on Earth is dominated by micrometeorites (MMs), cosmic particles between 10 µm and 2 mm in size (Genge et al., 2008; Zolensky et al., 2006; Suttle and Folco, 2020). The majority

of the MMs are interpreted to derive from asteroids in the main asteroid belt, similar to meteorites, although since they originate from different production mechanisms and transportation paths, the MMs sample parent bodies different from the larger meteorites (e.g., Engrand and Maurette, 1998; Flynn et al., 2009; Gounelle et al., 2009; Dartois et al., 2013; Cordier and Folco, 2014; Rubin, 2018). Micrometeorites are classified based on the degree of thermal reprocessing during atmospheric entry (Genge et al., 2008) with completely melted particles, termed cosmic spherules (CSs), representing the largest fraction of MMs (> 90 %) that are further classified based on their composition and textures (Genge et al., 2008; Taylor and Harvey, 1998; Toppani et al., 2001; Folco and Cordier, 2015). Contrary to Antarctic, deep-sea or urban roof collections, so-called "fossil" MMs are recovered from sedimentary rocks, and thus provide constraints on the past ET flux to Earth (Onoue et al., 2011), the timing of asteroid family formation (Heck et al., 2008) and the past composition of the Earth's upper atmosphere (Tomkins et al., 2016).

However, most ET material does not survive geological timescales and the occurrence of pristine MMs is rare (Tomkins et al., 2016; Dredge et al., 2010; Voldman et al., 2013; Suttle et al., 2023). Thus, fossil MMs have been documented in only 10 collections so far, but the reported extraction methods differ and display variable degrees of success (Suttle and Genge, 2017). Determining variations in the ET flux to Earth's surface over geological time is further complicated by the fact that the conventional proxies used to assess these changes are based on the much more rare, large-scale events recorded in the sedimentary record, such as (i) elevated iridium concentrations and/or decrease in osmium isotope ratios $^{187}Os/^{188}Os$ (*e.g.*, distal ejecta layer from the impact of the Chicxulub meteorite at the Cretaceous-Paleogene boundary) (Hildebrand et al., 1991; Goderis et al., 2021; Schulte et al., 2010), (ii) increase of ^{3}He (*e.g.* late Miocene and late Eocene), or (iii) increases in the abundance of rare ET spinel grains (Terfelt and Schmitz, 2021). The best-known example of the latter is an increase in the abundance of ET spinel grains in the geological record following the mid-Ordovician break-up of the L chondrite asteroid parent body (Suttle and Folco, 2020; Alwmark et al., 2012; Schmitz et al., 1996; 1997; 2014; Meier et al., 2010; Schmitz and Häggström, 2006; Greenwood et al., 2007). This break-up is thought to have led to a 100 to 1000-fold increase in the flux of MMs (Schmitz et al. 2019b), but also meteorites, as recorded by the occurrence of fossil meteorites in the Thorsberg quarry of Southern Sweden (Schmitz et al., 2001). As spinel group minerals represent ET material highly resistant to alteration and atmospheric entry, they have been applied as proxies to assess the ET flux in sedimentary records in recent years (e.g. Schmitz et al., 2019a), particularly using large (> 63 μm) chromite ($FeCr_2O_4$) mineral phases. Recent studies describe differences in the abundance and triple-oxygen isotopic compositions of the chromites recovered from sedimentary sequences before and after 466 Myr, interpreted to record a major change in the ET flux (Heck et al., 2010; Heck et al., 2016; Heck et al., 2017). Based on their triple-oxygen compositions and elemental compositions, the mid-Ordovician chromites have been linked to their potential parent bodies, chiefly represented by L-chondrite ordinary chondrites (OC) (e.g. Schmitz et al., 2019a; Heck et al., 2017; Alwmark et al., 2012), which represent only 17 % of the modern ET flux (Van Maldeghem et al., 2023). In modern MM collections, OC are only present in the larger size fraction (> 500 μm), while the most abundant size fraction (< 300 μm) is dominated by CS related to carbonaceous chondrites (CC) (Folco and Cordier, 2015). To extend our current understanding to the smaller size fractions of the cosmic dust flux, fossil micrometeorites represent a valuable addition. Despite their friable nature and challenges to extract from sedimentary rocks, recent work has shown that their extraction and study can provide priceless clues on the nature of the ET flux arriving to Earth through time (e.g. Suttle and Genge, 2017; Suttle et al., 2023).

Estimations of the ET flux variation in abundance and composition is currently limited to data from collections with relatively short accumulation windows (≤50 ka old, up to 1-3 Ma for sedimentary trap deposits, such as those described in Antarctica; Rochette et al., 2008; Goderis et al., 2020) and based on MM populations with large average diameters between 200 and 400 μm. Consequently, as each of the current individual proxies carry their own biases, no consistent reconstructions of the global ET

flux through time have been compiled so far. As such, accessing the complete ET flux, including fossil micrometeorites, is necessary in order to understand the nature of changes in the magnitude and composition of this ET influx to identify source materials and mechanisms. In addition, periods during which the ET material flux to Earth is higher than normal could be used to (i) reconstruct the past atmospheric composition based on the oxidation of cosmic spherules (CS) during atmospheric entry (e.g. Pack et al., 2017; Fisher et al., 2021) and (ii) trace the effects the flux may have had on the past climate, atmosphere and/or biosphere through atmosphere opacity, nutrient supply, and aerosol abundance (Lindskog et al., 2017; Reiners and Turchyn, 2018; Schmitz et al., 2019b; Rudraswami et al., 2021).

The present study provides the first fossil MMs collection recovered from late Devonian samples from the Latest Famennian ~ 360 Myr ago (Becker et al., 2020), representing an additional proxy to investigate the compositions and abundance of the past ET flux to Earth, through one of the largest major element and triple oxygen isotopic compositions data set of fossil MMs to date, with 1,222 fossil CSs extracted in the current study. This collection includes three well-preserved types of CSs, with a large iron-rich (I-type) CS collection, the oldest confirmed silicate-rich (S-type) CSs, and glass-rich (G-type) CSs, composed of silicate glass and magnetite dendrites. The alteration history of the spherules provides insights into the environmental conditions during the late Devonian and subsequent burial, as well as the extent of terrestrial overprinting. Oxygen isotope ratios are used to trace the primary origin of the recovered particles and may serve as a novel proxy for assessing Earth's atmospheric oxidizing capacity during that time.

II. Methods

II.1. Sampling site

The Chanxhe record (classically called Chanxhe I), located at the north-eastern border of the Dinant Synclinorium, encompasses the Comblain-au-Pont Formation, corresponding to the Latest Famennian (also called Strunian). The sedimentary rocks from this period are predominantly composed of sandy carbonate deposits alternating with shales, indicative of a deposition in a mixed littoral–marine setting, for the the Strunian Comblain-au-Pont Fm. (Denayer et al., 2021). Towards the top of the Formation, the proportion of detrital quartz tends to decrease, and this pattern is interpreted as related to a transgressive evolution through the Comblain-au-Pont Formation (Denayer et al., 2019). Through the studied section and the uppermost Famennian, distinct cyclic patterns are evident, featuring alternating layers of carbonate and siliciclastic deposits approximately 0.8 meters thick (Denayer et al., 2019). The final thick shale layer is dark in color and includes pectenid bivalves, indicating dysoxic conditions (Denayer et al., 2019) and interpreted as Hangenberg extinction event equivalent (Denayer et al., 2021). The Devonian-Carboniferous boundary itself is not visible in the Chanxhe I section, because the topmost part of the Comblain-au-Pont Formation is interrupted by a fault. The rock fragments used for the extraction of fossil micrometeorites are carbonates, selected for methodological consistency, and sampled from a 30 m stratigraphic interval, deposited at average sedimentary rates of 2.5 cm/kyr, which remain relatively constant throughout the studied section. The observed lithology is relatively homogeneous across the sampled intervals and lacks sedimentary features typically. The major element composition of powdered samples of the host rocks were analyzed using M4 Bruker Tornado µ-XRF analyses at the Vrije Universiteit Brussel (VUB), with a Rh X-ray tube, with 10 spots per sample with a spot size of 200 µm. In this study, around 30 kg limestone was sampled, representing an interval of <2 Myr from 7 intervals. Based on X-ray fluorescence analysis, the limestone intervals are on average composed of 86.7 wt% of $CaCO_3$ and 6.42 % of SiO_2, with some minor FeO (2.53 wt%), Al_2O_3 (1.15 wt%), MgO (2.53 wt%), and K_2O (0.33 wt%).

II.2. Extraction methods and initial classification

Micrometeorites (MMs) were extracted from limestone samples using a combination of mild acid dissolution, magnetic separation, and manual picking under optical microscopy. The carbonates rocks were cut into ~5 cm blocks (~125 cm3 each) and dissolved in HCl 15% (~4.5 M) until effervescence ceased, indicating complete decarbonation. The digestion process typically took between 7 and 12 days, depending on the sample composition. In total, 26 kg of carbonate material were processed, yielding approximately ~1.8 kg of residue. The residue was rinsed with Milli-Q water, and sieved in 6 distinct size fractions (32-63 µm, 63-125 µm, 125–200 µm, 200–400 µm, 400–800 µm, 800–2000 µm, and >2000 µm), and subsequently dried overnight. The magnetic fraction was separated by hand using a neodymium N45 (NdFeB) magnet. Following this, the magnetic spherules were selected based on exterior characteristics using a Zeiss Stereoscope Discovery V.20 optical microscope at the VUB. Only spherules exhibiting the characteristic features of CSs (as described in Folco and Cordier, 2015) were retained. These include spherical morphology, with an opaque metallic luster, matte sheen, or dark brown/black glassy shine. The focus was placed exclusively on CSs, as unmelted (and scoriaceous) MMs are considerably more difficult to differentiate from background sediments, and no fossil unmelted micrometeorites have been reported to date, as alteration and weathering could easily destroy them. The non-magnetic fraction was also examined to minimize potential biases introduced by magnetic separation and to recover potential non-magnetic MMs.

The extracted particles are mostly spherical with diameters ranging from 32 to 250 µm. The size distribution of the spherules is shown in Figure 1. A total of 388 MMs were selected to provide a representative overview of the observed surface textures, and include those with ambiguous exteriors. These selected particles were mounted in epoxy (EpoFix) resin, and polished using diamond paste (3 and 1 µm grain sizes) on a synthetic cloth, until a representative internal section was exposed. The polished mounts were carbon coated, and analyzed using a JEOL JSMIT300 scanning electron microscope (SEM) equipped with an energy-dispersive X-ray spectrometer (EDS) at the VUB. This allowed for the confirmation of their extraterrestrial origin, propose a classification, determine their state of alteration.

II.3. Geochemical analyses

A sub-population of 108 confirmed extraterrestrial spherules was selected for quantitative wavelength-dispersive X-ray spectrometric (WDS) analysis using a field emission gun electron microprobe analyzer (EMPA) JEOL JXA-8500F at the Museum für Naturkunde in Berlin, Germany. These analyses were conducted to confirm their ET origin and support their classification (Table 1 and Table 2).). In addition, 42 terrestrial spherules were analyzed, as some were added as reference due to their characteristic terrestrial textures, while others were defined to be terrestrial after analyses (Fig. 7). All spherules were analyzed using a spot size of 10 µm, a beam current of 15 nA, with an accelerating voltage of 15 kV, and counting times of 20 s on the peak and 10 s for the background for all elements, except for Na and K, which were analyzed with counting times of 10 s on the peak and 5 s for the background to minimize the effect of alkali loss. For all spherules, 2 to 3 spots of 10 µm were analyzed (depending on the the particle size), and averaged to obtain a bulk composition for each spherule. In the case of specific interesting phases, the spot size was decreased to 1 µm to obtain compositional information. Intensities of all analyses were calibrated against natural minerals and glasses of the Smithsonian international standard suite (Jarosewich et al., 1980) and pure metals of the Astimex metal standard. All analyses were processed by the JEOL series operating system ZAF routine to minimize matrix effects. All measurements of the spherules and an overview of the mineral standards used can be found in the Supplementary Data.

II.4. High-precision oxygen isotopic measurements

The oxygen isotopic compositions of the spherules were determined using a Cameca 1270 E7 secondary ion mass spectrometry instrument at CRPG-CNRS in Nancy, France, applying a Cs^+ beam with 1 nA primary current and 15 µm beam spot on the sample surface. A mass resolving power of 2500 was applied for ^{16}O and ^{18}O to avoid the $^{16}OH^-$ interference in the ^{17}O peak. The electron multiplier was used to measure ^{17}O, and Faraday cups in multi-collection mode was used for secondary ^{16}O and ^{18}O ions were measured using. Matrix-matched reference materials (San Carlos olivine, JV1 diopside, BHVO magmatic glass, UWCr chromite and CAF magnetite) were measured at the start and end of each analytical session to calculate the instrumental mass fractionation line, to correct for the instrumental mass fractionation due to matrix effects, and to check the stability and reproducibility of the isotopic data throughout the session. Oxygen isotope ratios are reported in standard δ notation, $\delta^{18}O$ is calculated as $\delta^{18}O = [(^{18}O/^{16}O)_{sample}/(^{18}O/^{16}O)_{ref} - 1] \times 1000$ (‰) and $\delta^{17}O$ using the $^{17}O/^{16}O$ ratio, relative to the Vienna Standard Mean Ocean Water (V-SMOW). The expanded 2σ uncertainties are ≈0.4‰ for $\delta^{18}O$, for $\delta^{17}O$, and ≈0.5‰ for $\Delta^{17}O$. The deviation from the TFL is expressed as $\Delta^{17}O = \delta^{17}O - 0.52 \times \delta^{18}O$ (Clayton, 1993). All measurements of the spherules can be found in the Supplementary Data.

III. Results

III.1. Petrography : textures and mineralogy

In total, 1,222 MMs have been identified from the 26 kg of carbonates. Most of those spherules are I-type MMs (92 % by number of the extracted spherules), G-type particles constitute around 6% of the extracted spherules, while 2 % is S-type. An intermediate subgroup, the G/I-types representing < 1 % by number was also established, for those spherules that could not be assigned to any of the other categories based on their textural and major element characteristics, especially in old fossil MMs that underwent terrestrial alteration.

I-type and G/I-type spherules

The I-type MMs (n= 1104) can be divided into metal-bearing (MET), or fully oxidized (OX) (Genge et al., 2017a). The MET spherules contained a metal bead (spherule S2M1B65, Fig. 2A), displaying a spherical cavity interpreted as a former metal bead (Van Ginneken et al., 2016; Suttle and Genge, 2017) (spherule S1M7C2, Fig. 2F) or a homogenous wüstite composition (spherule S1M7aa; Fig. 2C) (Fig. 2C). The oxidized spherules contain primarily magnetite with traces of remnant wüstite. I-type spherules display a continuum in wüstite/magnetite ranging from pure wüstite (FeO) to pure magnetite (Fe_3O_4), although most spherules are mainly composed of magnetite. In between the dendrites of magnetite/wüstite, the I-types fossil MMs show minor interstitial silicate material.

A number of spherules (n= 9) show a texture sharing characteristics intermediate between the I- and G-type types (Fig. 2D-E). They show a high abundance of magnetite dendrites, with interstitial silicate material, with finer dendrites resembling a G-type texture. These particles are classified into a new subtype, the G/I-types, as their texture, as well as composition (see the following section) are intermediate between the two groups, and does not allow a clear distinction.

G-type spherules

G-type spherules (n= 78) show dendritic magnetite in a silicate glass matrix. This group displays the largest variety of textures, in terms of dendrite shapes and abundance of glass (Fig. 3). Here, the fine dendritic G-type particles (Fig. 3A), showing fine sub-micron magnetite dendrites with the interstitial

material are distinguished from the bulky dendritic G-type spherules with magnetite dendrites up to 10 µm of thickness, with larger pockets of interstitial silicate material (Fig. 3D) and medium dendritic G-type particles, exhibiting more conventional µm sized dendrites in silicate glass (Fig. 3B). These 3 subcategories form a continuum, with some spherules showing a mixture of the described characteristics (S3M1B23 Fig. 3C).

S-type spherules

From the sediments, 32 S-type spherules were extracted (Fig. 4). The S-type spherules are composed of silicate phases mainly. Following approximately 360 Myr of terrestrial weathering, most fossil MMs did not preserve their initial texture or composition. However, 4 extracted spherules appear to have been preserved from extensive weathering (termed "Mg-rich S-types" in this study), and retained their barred olivine (BO) texture, showing parallel micrometers-thick Mg-rich olivine, and nanoscale magnetite crystallites within an interstitial silicate mesostasis (S2M1A11, S2M1A2, S2M1A15, S5M1C13, Fig. 4A-C). The 11 other silicate spherules display more weathering (termed the "Mg-poor S-types"), with slight replacement of the initial texture by secondary minerals, as most of the initial olivine and/or silicate glass have recrystallized into phyllosilicates following aqueous weathering (Fig. 4D-I).

A set of spherules (Fig. 4D-I) (n= 18) shows fine-grained cryptocrystalline (CC) texture and composition, characterized by sub-micron sized crystallites of Fe-rich olivine (partially replaced by phyllosilicates), arranged in feather-like skeletal crystals, with nano-scale magnetite, in interstitial glass. They show small magnetite dendrites within silicate phases, and some weathered texture (recrystallized to palagonite). Two spherules display a relict porphyritic (PO) texture (S4M1A34, S4M1A56 Fig. 4E), with silicate micro phenocrysts (weathered Fe-rich olivine) with no preferential direction, and magnetite within a silicate glass mesostasis. Finally, 7 spherules have a glass V-type texture, with homogenous silicate glass (Fig. 4D).

III.2. Elemental compositions

In a ternary diagram SiO_2 vs. MgO vs. FeO (Fig. 5), the bulk compositions of the spherules describe a continuum between the I-, G-, and S-type spherules, while all terrestrial spherules plot closer to the SiO_2 endmember composition. Using the combination of textural observations and elemental compositions, particles from the different type groups were identified. In addition, a subgroup G/I-type cosmic spherules are added to describe spherules showing ambiguous textures and elemental composition.

I-type and G/I-type spherules

The I-type spherules are mainly composed of magnetite-wüstite iron oxides. The FeO content ranges from 68.6-97.6 wt%, with average 86.2 ± 0.7 wt%. The atomic Fe/Si ratios range from 9.77 to 73,989 depending mostly on the abundance of interstitial silicate glass. The MgO content reaches up to 0.92 wt%, with an average of 0.09 ± 0.19 wt%. The Mg content is linked to the abundance of interstitial silicate glass (Table 1). The NiO content is up to 3.73 wt%, with average of 0.12 ± 1.43 wt%, Cr_2O_3 < 4.07 wt%, averaging 0.31 ± 0.69 wt%. Minor (< 1 wt%) Ti, V and Zn concentrations are observed in some spherules. The MnO content is < 2.79 wt%, with an average of 0.47 ± 0.61 wt%; CaO < 3.12 wt%, with an average of 0.23 ± 0.56 wt%; Al_2O_3 is < 2.01 wt%, with an average of 0.36 ± 0.55 wt%.

One I-type spherule (S2M1B65, Fig. 2A) contains a preserved $Fe_{80}Ni_{20}$ metal bead (taenite), surrounded by magnetite containing Cr_2O_3 (1.43 wt%), NiO (3.73 wt%) and SO_3 (0.69 wt%) (all detailed data are available in Table S1). One I-type spherule (S1M11C21, Fig. 2B) has an inclusion of ferrihydrite, created by terrestrial weathering of a metal bead (Genge et al., 2017a). This spherule also contains both

wüstite and magnetite. The interior of the spherule appears to be pure wüstite, with a gradual oxidation towards the rim changing into magnetite. The magnetite is observed in the rim all around the spherule with a thickness of around 2 µm. Finally, one I-type spherule (S1M12A34) displays a corundum inclusion within magnetite (Fig. S1). The oxide mineral is around 25 x 10 µm with rounded margins and is largely composed of Al_2O_3 with a minor presence of TiO_2 and FeO (0.13 wt% and 0.59 wt% respectively).

The G/I-types have composition in between G- and I-types. They show high Fe/Si ratio from 6.26 to 10.37, FeO from 72.01 to 84.48 wt%, and SiO_2 6.57-10.50 wt% and low Al_2O_3 <3.19 wt% (Table 1). Indeed, S3M1A55 is classified here as a G/I-types (Fig. 2D), and and shows (i) a relic of a FeNi spherule, recrystallized into a I-type like spherule FeO (87.62 wt%) with high NiO (0.44 wt%), (ii) surrounded by a G-type like texture and composition with SiO_2 (16.7 wt%), FeO 66.8 wt%; Al_2O3 (3.64 wt%), CaO of (7.33 wt%), MgO (0.80 wt%), P_2O_5 (1.11 wt%) (Table S1).

G-type spherules

G-type cosmic spherules are mainly composed of magnetite and silicate glass (Table 1, Fig. 3, Fig. S2). Their bulk composition ranges from 10.9 to 41.8 wt% SiO_2, with an average of 25.9 ± 15.1 wt%; 19.0 to 72.6 wt% FeO, with an average of 48.4 ±15.1 wt%; 3.20-22.95 wt% Al_2O_3, with an average of 9.39 ± 4.29 wt%; 0.02-9.83 wt% MgO, with an average of 1.72 ± 2.58 wt%; and 0.07-7.78 wt% CaO, with an average of 2.07 ± 1.97 wt%. G-type spherules contain trace of TiO_2 (average of 0.72 ± 0.65 wt), MnO (0.32 ± 0.71 wt%), P_2O_5 (0.21 ± 0.19 wt%), and ZnO (0.03 ± 0.02 wt%). The NiO content is low < 0.08 wt%, with an average of 0.02 ± 0.02 wt% and Cr_2O_3 < 0.14 wt%, with an average of 0.02 ±0.02 wt%.

The glass phase of G-types was measured for 4 spherules where surface of glass where large enough to be properly analyzed with minimal interference of surrounding magnetite, giving average composition of SiO_2 47.95 wt%, Al_2O_3 18.84 wt%, FeO 15.45 wt%, CaO 6.03 wt%, TiO_2 2.85 wt%, P_2O_5 0.77 wt%, MgO 0.75 wt% and MnO 0.66 wt%. The magnetite in G-types have composition of FeO 84.1 wt%, SiO_2 1.46 wt%, Al_2O_3 2.19 wt%, MnO 0.71 wt%, MgO 0.51 wt%, CaO 0.24 wt%, TiO_2 0.42 wt%, and NiO 0.26 wt%. Some G-types have high Mg composition (MgO > 4.00 wt%) : S2M1A16 (4.11 wt%), S2.5M1B510 (9.83 wt%), S4M1C11 (9.43 wt%), S5M1B21 (7.18 wt%), S3M1B43 (5.08 wt%) (Table 1, Table S1). Most compositions describe a continuum in the G-types, although S2.5M1B63 and S3M1A15 (Fig. 3D) show unusually high TiO_2 abundance (average 2.53 and 3.10 wt% respectively).

S-type spherules

The S-type spherules extracted in this study can be divided into two subgroups : (i) the Mg-rich, and (ii) Mg-poor subgroups (Table 2). The Mg-rich S-type cosmic spherules exhibit astonishing preservation, with a high content of MgO (ranging between 20.0 and 31.8 wt%, and an average of 27.0 ± 4.91 wt%) and NiO (between 0.03 and 1.62 wt%, with an average of 0.89 ± 0.57 wt%), in addition to the expected SiO_2 (34.0-43.7 wt%, with an average of 37.6 ± 3.87 wt%) and FeO (15.6-35.0 wt%, with an average of 26.6 ± 7.39 wt%). They show a low content of Al_2O_3 (1.23-3.36 wt%, averaging 2.51 ± 0.80 wt%) and a content of TiO_2 (0.13 ± 0.02 wt%), Cr_2O_3 (0.29 ± 0.13 wt%), MnO (0.35 ± 0.06 wt%), and CaO 2.53 ± 0.54 wt%), with low Na_2O+K_2O (0.01-0.24 wt%). The Mg-poor S-type spherules show a lower content of MgO (0.08-2.51 wt%, average of 0.80 ± 0.54 wt%) and NiO (<0.07 wt%, average of 0.02 ± 0.01 wt%), and higher Al_2O_3 (2.33-32.4 wt%, average of 16.9 ± 6.89 wt%). Mg-poor S-type spherules also display lower Cr_2O_3 (0.02 ± 0.01 wt%), MnO (0.13 ± 0.18 wt%), with slightly higher TiO_2 (0.69 ± 0.42 wt%) and Na_2O+K_2O (1.12 ± 0.51 wt%). They exhibit a composition similar to that of the main G-type composition in terms of SiO_2, FeO and CaO.

III.3. Size distribution

For the 1,222 extracted MMs, 70.4 % by number are in the 32-63 µm size fraction, 26.2 % in the 63-125 µm size fraction and 3.2 % fall in the 125-200 µm size fraction (Fig. 1). The diameter of each particle was calculated based on the measurements of the axes (the long axis a and short axis b), with the formula $\sqrt[3]{axb^2}$ (Suavet et al., 2009). Only 3 spherules exhibit a diameter (average diameter measured from SEM images) above 200 µm (1 G-type and 2 I-type particles) (Fig. 1). The I-type and G-type cosmic spherules are found in all size ranges (32-250 µm). The more silicate-rich spherules (S-type cosmic spherules) are found only in the smaller size fraction (< 125 µm). In previous studies, power law fits have been applied to specific size fractions of micrometeorite collections to assess potential biases from sampling, accumulation, or terrestrial alteration (e.g., Taylor et al., 1998, 2000, 2007; Fig. 1). For example, analyses of the South Pole Water Well (SPWW) consistently yielded slope values between −5.1 and −5.2 in the 200–700 µm size range. These values are considered representative of an unbiased cosmic dust flux to Earth (Taylor et al., 2000). More recently, deviations in slope profiles have also been interpreted as evidence for multiple dust sources with distinct size distributions (Suttle and Folco, 2020). The fossil CSs extracted from the late Devonian carbonates have consistent slopes around -3.26 for I-types, -3.30 for G-types, and -3.08 for S-types (Fig. 1).

III.4. Triple oxygen isotopic composition

The $\delta^{17}O$, $\delta^{18}O$ and $\Delta^{17}O$ values for 160 spherules are reported in Table S2. In total, 87 I-type, 4 G/I-type, 43 G-type, and 26 S-type have been measured for oxygen isotope ratios (Table 3). These spherules were selected based on limited degrees of weathering. At present, this represents the largest triple oxygen isotope data set for fossil MMs, and includes abundant fossil silicate-rich CSs (G-type and S-type particles).

In Fig. 6, the $\Delta^{17}O$ versus $\delta^{18}O$ are plotted relative to the terrestrial fractionation line (TFL) and the oxygen isotopic compositions of the main chondrite groups (Clayton et al., 1991; Clayton and Mayeda, 1999; Newton et al., 2000). The triple oxygen isotopic compositions of the extracted spherules are compared to the four CSs groups defined qualitatively by Suavet et al. (2010) (Fig. 6).

I-type and G/I-type spherules

In the case of the analyzed fossil I-type CSs, 12 I-type spherules plot above the TFL, falling within or close to the Group 3 field, and show $\Delta^{17}O$ values between 0.1 and 1.0‰ and positive $\delta^{18}O$ values (Suavet et al., 2010). In total, 23 I-type and 1 G/I-type spherules plot below the TFL. Three of the I-type spherules exhibit isotopic compositions that can be linked to the Group 1 field, and present $\Delta^{17}O$ below -2.2‰ and $\delta^{18}O$ in the range of 8 to 32‰ (Suavet et al., 2010). One spherule (S6M1C55) plots close to meteoritic CM values with a lower $\delta^{18}O$ of ~2.1‰, and is also associated with Group 1. In addition, 4 I-types and 1 G/I-type plot within the Group 2 values with $\Delta^{17}O$ between -0.2 to -1.5‰ and $\delta^{18}O$ ~25‰ (Suavet et al., 2010). Spherule (S2M1B65) shows slightly positive $\Delta^{17}O$ values above the TFL (0.45‰) and high positive $\delta^{18}O$ (51.3‰) close to some Antarctica Group 4 spherules (Lampe et al., 2022). This spherule could potentially be linked to an extended ^{16}O-poor Group 4, characterized by positive $\Delta^{17}O$ and $\delta^{18}O$ ≥40‰ (Suavet et al., 2010). Three I-type spherules have $\Delta^{17}O$ values falling in between Group 1 and Group 2 and cluster closer to meteoritic values with $\Delta^{17}O$ between -2.2 and -1.5‰ and $\delta^{18}O$ ~3.7-7.4‰. In addition, 8 I-types show values close to CR(-CM) meteoritic values, with $\Delta^{17}O$ between -0.5 to -1.5 and $\delta^{18}O$ of 0.16-7.2 ‰.

G-type spherules

Based on our analyzed CSs, 28 G-type spherules can be resolved from the TFL and fall below the TFL line. Seven spherules plot within the Group 2, while 8 spherules plot close to Group 2 values with

lower $\delta^{18}O$, falling close or in the CR meteorites field ($\delta^{18}O$ of 8.35 to 17.7‰). Two spherules fall within Group 1 values, while 8 spherules overlap with the CM field with lower $\delta^{18}O$ (5.57 to 11.7‰). Four of the analyzed G-type spherules display more negative $\Delta^{17}O$ (-5.71 to -8.40‰) (S2M1A3, S2M1A65, S2M1A71, S3M1C15). Those spherules are not linked to any MM fields or bulk meteorite groups.

S-type spherules

Of the 26 S-types measured, there are 15 S-type spherules that show values resolved from and below the TFL. Five S-type (CC-type) and 1 S-type (BO-type) plot within or close to the Group 2 values ($\delta^{18}O$ of 15.44 to 30.37‰ and $\Delta^{17}O$ of -0.60 to -1.86‰), one S-type (BO-type) plots near the Group 2 but within the CR meteorite field ($\delta^{18}O$ of 8.56‰ and $\Delta^{17}O$ of -0.50‰). Three S-types (CC) plot close to Group 1 values, closer to CM/CV meteorite values ($\delta^{18}O$ of 4.14 to 14.3‰ and $\Delta^{17}O$ of -2.21 to -2.61‰). Finally, 2 S-type spherules (CC-type S2M1A45 and S2M1A46) and 2 S-type particles (V-type S2M1A51 and CC-type S2M1A66) plot below Group 1 values, with negative $\Delta^{17}O$ (-4.71 to -7.34‰), and low $\delta^{18}O$ (-1.60 to 6.17‰). Similar to several G-type particles, these spherules cannot be linked to any MM fields or bulk meteorite groups.

III.5. Other particles

In addition to the CSs, several other terrestrial particles were picked out, due to their unusual physical properties and optical resemblance to MMs (Fig. 7). Internally, these particles display aggregates of FeS_2 microcrystallites, with aqueous alteration into iron (hydr)oxides: magnetite, hematite, and goethite. Additionally, polymineralic magnetite grains were observed, characterized by irregular morphologies and fibrous textures (Fig.7). These features are indicative of fluid-mediated growth or alteration (Fig. 7) and contrast with the fast-cooled textures of iron oxide-rich I-types and G-types MMs. Their chemical compositions also differ significantly, consisting of combinations of iron oxides, hydroxides, and sulfides, and notably lacking diagnostic elements such as Ni, Co, or Cr. This clearly distinguished them from iron oxide-rich MMs, primarily composed of wüstite and/or magnetite (Table 2).

IV. Discussion

IV.1. Terrestrial versus extraterrestrial spherules

The first challenge when extracting fossil MMs is to distinguish them from terrestrial spherules that could resemble MMs, such as volcanic particles, terrestrial iron rich spherules or weathered silicate spherules. Generally, fossil MMs show an increase in textural and compositional alteration and/or replacement by secondary phases with increasing age, increasing the number of fossil MM that can be mistaken to represent terrestrial particles. Here, a method to distinguish the MMs from potential terrestrial particles using texture and major element composition is discussed. Given the strict set of criteria applied, there is a risk that MMs may be excluded that are too altered to differentiate from alike terrestrial spherules. All estimates reported here can thus be considered as minimal values. Texture is the primary characteristic used to distinguish between terrestrial and ET spherules (Figs. 2-4). After embedding and polishing of the spherule interiors, SEM analyses revealed several types of terrestrial iron-oxides, iron-hydroxides and sulfides, which exhibit textures that unambiguously differentiate them from iron-oxide rich ET spherules, the I-type and G-type MMs (Fig. 7). In addition to their distinct textures, these terrestrial spherules, composed of iron-oxides combined with iron-hydroxides and sulfides, exhibit compositions that differ significantly from MMs, which are primarly composed of wüstite and/or magnetite.

For silicate spherules, ET particles are challenging to differentiate from silicate-rich terrestrial particles based solely on their texture. Certain terrestrial spherules closely mimic altered micrometeorites, with weathering further obscuring the original texture of potential silicate cosmic spherules (CSs) through processes such as the recrystallization of silicate glass into palagonite (Van Ginneken et al., 2017). Consequently, the major element composition is used to confirm the ET origin of the spherules. The spherules exhibit Ni contents < 3.73 wt% NiO in bulk analyses, with a single-point analysis reaching 10.82 wt% NiO in an Fe-Ni bead within the I-type spherule S2M1B65 (Fig. 2A, Table 1). While the presence of Ni supports an ET origin for some spherules (NiO > 0.5 wt%, as terrestrial glass/olivine typically shows a maximum of 0.5 wt% NiO; Sahu et al., 2020), the overall low content of Ni content (NiO < 0.5 wt%), likely caused by leaching during terrestrial weathering, limits its reliability as a general discriminative parameter. Similarly, the Cr_2O_3 content remains below 4.07 wt%, making it unsuitable as a distinguishing criterion.

On a plot of Na2O + K2O abundances versus Fe/Si ratio (Fig. 8A), the terrestrial and ET spherules occupy different regions of the diagram. We included terrestrial particles with clearly recognizable terrestrial textures and compositions (e.g. glassy and quartz-rich, with high K_2O and Na_2O content), confirmed ET spherules (notably barred olivine textures with high nickel content), and ambiguous spherules to visualize the composition fields and potential overlaps. Terrestrial spherules display Na2O + K2O contents ranging from 0.96 to 7.41 wt%, with an average of 2.87 ± 1.43 wt%, whereas ET spherules consistently plot below 2.10 wt%, with an average of 0.94 ± 0.59 wt%. In terms of Fe/Si ratios, terrestrial spherules range from 0.03 to 0.67 (average 0.25 ± 0.13), while the ET spherules span a wider range, from 0.30-20.6, with an average of 4.45 ± 4.92. These values remain higher than those typically observed in Antarctic micrometeorites, which average ~0.13 wt% $Na_2O + K_2O$ (Goderis et al., 2020), suggesting that the Chanxhe spherules experienced more intense or compositionally different terrestrial alteration—likely due to interactions with the clay-rich carbonate host rock. Even if some spherules plot near the boundary between the ET and terrestrial fields, these can be resolved by combining their composition and textural observations.

IV.2. Chemical exchange of metal – magnetite and wüstite: I-type and G-type cosmic spherules

The identified I-type CSs possess all required characteristics of modern-day I-type spherules with their small sizes (< 400 µm), the quenched dendritic textures, the presence of intact metal beads or internal cavities from dissolved metal beads, their high-temperature oxidized mineralogy (wüstite-magnetite), and the occurrence of Ni-rich wüstite (Genge et al., 2017a; Suttle et al., 2023), despite the extensive terrestrial alteration experienced by some of the particles during their long terrestrial residency.

The least altered CSs are found in Antarctic and urban MM collections (e.g., Taylor et al., 1997; Duprat et al., 2007; Genge et al., 2017b; Goderis et al., 2020; Suttle et al., 2021). I-type spherules are classified into metal-bearing (MET) and oxidized (OX) subtypes (Genge et al., 2017a) and typically compose ~3 % (range <1 up to 10 %) of all cosmic spherules (Van Ginneken et al., 2024). Those I-types are formed following melting and oxidation of droplets of chondritic metal (kamacite and taenite) during atmospheric entry (Genge et al., 2017a). Under current atmospheric conditions, this leads to continuum of oxidized spherules, from a layered internal structure encapsulating a metal bead within a metal-oxide shell (MET), to a fully oxidized spherule with no remaining metal bead (OX). The crystallization of oxidized metal results in the formation wüstite. The different oxidation potential of Ni (higher) and Fe (lower) causes a difference of Ni content between a more Fe-enriched shell and metal beads enriched in Ni (Suttle et al., 2023). This results in I-type spherules being composed of mainly Ni-poor magnetite: MET I-type particles with Ni-poor (<1.5 wt%) wüstite and minor Ni-free magnetite as rim; and OX I-types with Ni-richer (0.5-22.5 wt%) wüstite and more abundant Ni-free magnetite (Genge et al., 2017a).

Compared to the more pristine, modern-day collections, the extracted fossil I-type spherules from Chanxhe have lost most of their Ni (0.12 wt% Ni on average) and Cr (0.31 wt% Cr on average) (Table 1). Our spherules generally display Ni-poor compositions. In MET spherules, this reflects a lower degree of oxidation, with Ni retained in a central metal bead while the surrounding magnetite remains Ni-free. However, during terrestrial residence, this metal bead is often weathered—either completely leached out or altered into Fe-hydroxides. In contrast, OX spherules—formed under higher oxidation conditions—initially contain Ni-bearing magnetite, but terrestrial alteration may also lead to Ni loss through leaching (Table 1; Genge et al., 2017a; Suttle and Genge, 2017). The presence of Na, Mg, Al, Si, Ca, Ti and Mn can also be observed in the extracted I-type CSs, and can be explained by silicate amorphous material in interstitial space of the iron-oxides (Table 1) (Fig. 8C). This interstitial amorphous material can either be produced by terrestrial alteration fluid circulation and deposition within void spaces between magnetite dendrites (Suttle et al., 2023), or by alteration of pre-existing glass in the interstitial magnetite (strengthening the observed continuum between G-type and I-type textures) (Fig. 8B). One spherule (Fig. 2D) shows an unusual texture, featuring an iron-oxide core enriched in Ni with a silicate-rich, iron-bearing rim, which likely reflects a metal droplet that experienced extensive oxidation during atmospheric entry. Such a feature could suggest localized chemical exchange between metal and silicate phases, possibly driven by large-scale oxidation, resulting in iron partitioning into the surrounding silicate matrix—an uncommon but insightful record of the spherule's complex alteration history. In addition, Mg^{2+}, and Al^{3+} (lithophile cations) can also be implanted into the Fe-oxide (magnetite/wüstite) crystal structure during alteration, with little changes in the lattice structure (Suttle et al., 2023), explaining the presence of these elements in the bulk analyses of I-type and G-type spherules. On a plot of Al_2O_3 versus Fe/Si, both an increase in silicate content (lowering the Fe/Si) and more pronounced degree of terrestrial alteration (increasing the Al_2O_3 content in altered silicate phases and Fe-oxides) are observed, allowing the distinction between different MM types, as well as constraining the degree of terrestrial alteration (Fig. 8B).

Manganese is a lithophile elements, with Mn^{2+} cations compatible in the wüstite and magnetite structure substituting $Ni^{2+,}$ Fe^{2+} or other cations occupying divalent sites. Previous studies extracted I-type fossil MMs from deep sea sediments, in which the returned particles showed either no Mn-enrichment (Bonte et al. 1987; Rudraswami et al., 2014; Savelyev et al., 2022), or Mn-enriched magnetite. This indicates that Mn substitution can occur in deep-sea settings but is likely enhanced significantly during diagenesis (Agarwal and Palayil, 2022; Suttle et al., 2023). Therefore, high Mn contents in I-type fossil CSs have been described as a characteristic feature of altered fossil MMs that underwent diagenesis in marine settings (Suttle et al., 2023). Here, the recorded Mn concentrations are not as high as the previously observed in Mn-enriched fossil I-type CSs (0.47 ± 0.61 wt% Mn on average versus 4.27 wt% for marine CSs). The Chanxhe fossil MMs were extracted from a shallow marine environment, that did not lead to extensive Mn substitution due to less Mn available in the environment (average MnO 0.09 wt%), although the host rocks underwent some degree of diagenesis that can explain the increase in Mn in a set of spherules (maximum MnO of 2.79 wt%) (Force and Cannon, 1988).

IV.3. Chemical exchange and alteration of silicate and glass : G-type and S-type cosmic spherules

Silicate and glass weathering

Weathering of olivine rich S-type CSs has been observed in Transantarctic MMs, with dissolution leading to etch pits along faces of olivine crystals (van Ginneken et al., 2016). The best-preserved S-type fossil MMs extracted from Chanxhe, the Mg-rich spherules, only show minimal traces of dissolution along their edges (Fig. 4, Fig. 9). Their major element composition typically falls within the range of modern S-types from Antarctica (Fig. 8; Goderis et al., 2020), supporting their excellent state

of preservation. The Mg-rich S-type spherules are among the oldest preserved fossil S-type MMs recorded to date.

The Mg-poor V-type spherules show typical S-type textures (Fig. 4D). The V-type CSs have high concentrations in Al_2O_3 (> 13.2 wt%) and FeO (> 41.5 wt%) and show a content of MgO (<1.49 <t%), NiO (<0.04 <wt%), and Cr_2O_3 (< 0.02 wt%) (Table 2). These spherules are described as weathered V-type CSs, in which Fe- and Al-rich silicate glass homogenously weathered into Fe-rich palagonite, explaining the Al^{3+} enrichment (Fig. 8B). The high Fe content in the V-type fossil spherules might be explained by an initially higher Fe composition in the glass.

The fossil CC- and Po-type CSs show typical texture with some minor etching on the edges (Fig. 4). These spherules have compositions high in Al_2O_3 (23.5-32.4 wt%), with a loss of MgO (<0.68 <t%), NiO (<0.02 <wt%), and Cr_2O_3 (< 0.03 wt%) (Fig. 8B, Table 2). The composition shows replacement of Mg^{2+} by Ca^{2+} and $Fe^{2+/3+}$ by mainly Al^{3+}. The texture and bulk composition of the Mg-poor S-type CSs are similar to the altered S-type CSs found in Antarctica (Van Ginneken et al., 2016), or in meteorites (e.g. Gooding 1986), with crystallization of palagonite-type amorphous material mixed with nanoscale smectite phyllosilicates found in the micrometeorite (Fig. 4, Fig. 9).

Fossil G-type CSs show weathering pathways, resembling both those of I-type and S-type particles. Magnetite alters in the same way as I-type magnetite, with increases in Mg^{2+}, Ca^{2+} and Al^{3+} (lithophile cations) into the Fe-oxide crystal structure, as highlighted for the I-type particles (Table 1). Their silicate component undergoes weathering similarly as V-type CSs, characterized by high concentrations of Al_2O_3, SiO_2, and FeO coupled with low levels of MgO, NiO, and Cr_2O_3. This indicates hydration of the interstitial material and formation of Fe- and Al-rich palagonite (Fig. 8B, Table 1). The determined compositions and alteration patterns of the G-type CSs support the interpretation of a petrographic continuum between I-type to G-type to S-type CSs (Fig. 8B).

The silicate material in cosmic spherules of S-type (CC-type) is altered into palagonite, resulting in the loss of most or all of their original S-type textures, as observed in samples S2M1B53 (Fig. 4H) and S3M1A31 (Fig. 4I). Both exhibit a residual CC-type texture following replacement by secondary palagonite.

Comparison to chondritic composition

Studying fossil MMs and comparing their composition to chondritic values can be challenging as the leaching of major and minor elements (Mg, Si, Ni), and alteration of silicate phases (increase of Al, Si, Fe) strongly affects the bulk chemical composition (Table 1, Table 2, Fig. 8). In the case of 4 Mg-rich S-type the major element compositions are extremely well preserved, while 22 Mg-poor S-type particles show stronger effects of alteration in terms of texture and composition. The 4 preserved Mg-rich S-type CSs show chondritic Mn/Mg ratios with positively correlated Fe/Mg and Fe/Mn ratios (Fig. 8F). The Mg-poor S-type CSs have Mn/Mg above the chondritic ratio, with variable Fe/Mn ratios, distinct from the horizontal lines described for achondritic compositions (e.g., Soens et al., 2022). Spherules originating from differentiated parent bodies typically display consistent Fe/Mn ratios, but elevated Fe/Mg ratios compared to chondritic materials. They tend to plot along horizontal trends corresponding to the values observed for the Moon (Fe/Mn ≈ 75) or Mars (Fe/Mn ≈ 25) (Fig. 8F). The signatures of Mg-poor S-type CSs observed here is explained by originally chondritic values from which Mg was lost during weathering, leading to an extension toward higher Fe/Mg and plotting along a line that is shifted from extraterrestrial materials. Two S-type spherules (CC-type S2M1B4, S6M1C34) plot closer to “achondritic” compositions (Fig. 8F), although their Fe/Mn are higher than the expected ratios (Fe/Mn between 57-80).

On a plot of Si/Al versus Mg/Al, the values of the 4 Mg-rich S-type particles are positively correlated (Fig. 8E), attesting to minor to moderate degrees of weathering but also minor evaporation, similar to what is observed for a fraction of the modern CSs. The other S-type CSs plot lower and are offset from the evaporation trajectory, which reflects either more extreme atmospheric heating conditions, or alteration with leaching of Mg and increased Al, the latter of which is supported but the observed textures.

Based on the atomic Fe/Si ratio and CaO and Al_2O_3 contents, chondritic CSs have previously been assigned to three distinct chemical groups (Cordier et al., 2011) (Fig. 8D). Assuming minimal weathering effects on major element compositions, the Mg-rich S-type CSs and one S/G-type spherule (S2M1B53) plot within the 'normal' chondritic group, supporting their relatively well-preserved state (Fig. 8D). In contrast, the remaining S-type and S/G-type CSs plot within the high Ca-Al group, characterized by Fe/Si > 0.47 and CaO + Al_2O_3 > 9 wt%. This may reflect either their original composition or secondary enrichment in Ca and Al due to terrestrial weathering and interaction with the carbonate host rock.

IV.4. Evolution of the extraterrestrial flux

Size distribution and preservation biases

In the collection presented here, 96 % of the spherules have diameters below 125 µm (Fig. 1). Modern collection MM sizes peak at 210–330 µm (Genge et al., 2018), 200–250 µm (Taylor et al., 1998, 2000), and 265 ± 92 µm (Prasad et al., 2013). Suttle and Folco (2020) showed a bi-modal distribution with a peak around 250 µm (higher for Transantarctic Mountain region) and another peak at 145 µm (higher for Larkman Nunatak region). This could be explained by a bimodal signal of the general MM flux, with relative contributions of components varying at different site, with higher I-type component in the Larkman Nunatak region (Suttle and Folco, 2020). The smaller size of the spherules extracted in the collection can be explained by the composition as well as the age of the fossil MMs: (i) Fossil MMs typically show more I- (< 240 µm) and G-type CSs (<280 µm), which are on average smaller than S-type CSs based on modern collections (< 370 µm) (e.g., Suttle and Folco 2020, Tomkins et al. 2016). (ii) Dissolution and alteration of spherules can weaken their mechanical strength, making the larger particles more prone to fragmentation or dissolving. As a result, the relative abundance of smaller particles increases, leading to a passive enrichment of the smaller fractions (Van Ginneken et al., 2016). (iii) This size distribution may also reflect the original accretion flux, as recent modeling predicts a bimodal mass flux of cosmic dust with peaks at approximately 1-10 µm and 100-500 µm (Walton et al., 2024). In addition, particle loss may be assessed by comparing the cumulative size distribution of the fossil micrometeorite (MM) collection with those of more well-preserved collections (Fig. 1). For instance, the South Pole Water Well (SPWW) collection, considered largely unbiased, consistently shows steep slopes (exponents of approximately −5) in the 200–700 µm size range (Taylor et al., 2000). In contrast, the TAM and Larkman Nunatak collections yield shallower slopes (greater than −5), indicating the potential loss of more fragile particles (Suavet et al., 2009; Genge et al., 2018; Goderis et al., 2020; Van Maldeghem et al., 2024). An extreme case is observed for the Walcott Névé collection, which contains a high proportion of moderately to severely weathered MMs and a dominance of weathering-resistant I-type spherules, with a slope of −2.9 for the 200–400 µm fraction (Suavet et al., 2009). In comparison, the fossil MMs from this study show cumulative size distribution slopes ranging from −3.3 to −3.08 (Fig. 1), consistent with trends seen in altered Antarctic collections enriched in I-types. This suggests substantial weathering-related particle loss during burial, diagenesis, and terrestrial residency. However, direct comparisons are complicated by differences in accumulation time windows. Antarctic collections typically integrate particles accumulated over long exposure times, up to ~3 million years (Goderis et al., 2020). This allows the collection to acquire a broader size range and more diverse populations of cosmic dust, including both more recent and older particles. In contrast, the fossil MM samples studied here likely reflect accumulation over much

shorter time intervals (~10 kyr per sample), making them more susceptible to temporal gaps and the selective preservation of smaller and more chemically resistant particles.

Biases in cosmic spherule types

Silicate and glass with compositions close to olivine are the main constituents of modern-day S- and G-type spherules. Olivine is known to be easily weathered in the conditions prevalent at the Earth's surface, and can easily be leached and replaced by secondary minerals (e.g., Delvigne et al., 1979; Nesbitt and Wilson, 1992; Bland and Rolls, 1998; Stefansson et al., 2001). The low abundance in this study of silicate-rich spherules (S-type and G-type CSs (~ 9 %)) has previously been observed in studies that focused on fossil MMs extracted from marine sedimentary rocks in different stratigraphic intervals (e.g. Voldman et al., 2013; Tomkins et al., 2016; Kadyrov et al., 2020; Suttle et al., 2023). This is explained by weathering of silicate phases in marine and aqueous environment due to etching and dissolution during exposure to (sea)water (Nelson et al., 1995). In addition, the preferential removal of olivine, especially Mg-rich olivine, compared to glass, explains the general lack of S-type CSs and other olivine-rich CSs in fossil MM collections (e.g. Genge et al., 2008, Van Ginneken et al., 2016, Suttle et al., 2023). The low abundance of S-type particles from the late Devonian collection at Chanxhe (~ 2.6 %) thus reflects a passive increase of iron oxide-rich CSs (I-type and G-type CSs), which has also been observed in more recent marine MM collections (Murray and Renard, 1891; Blanchard and Davis, 1978; Murrell et al., 1980; Savelyev et al., 2022).

Composition of the cosmic spherule flux

Previous studies have extracted and studied fossil MMs to assess the past ET flux to Earth (e.g. Mutch 1965; Taylor and Brownlee, 1991; Onoue et al., 2011; Tomkins et al., 2016; Suttle and Genge, 2017; Kadyrov et al., 2020). In this study, we present one of the oldest preserved S-type fossil CSs and a rich collection with over 1,200 fossil CSs, making it one of the largest fossil MMs collection recovered to date. The presence of preserved S-type CSs coupled with the large abundance of G- and I-type spherules in this section could be explained by (a combination of) multiple factors.

(i) The applied extraction method is relatively gentle on the spherules and could have led to less damage during extraction, relatively to methods applying silicate dissolving acids (HF) and/or mechanical desegregation. This could lead to the recovery of more fragile fossil MMs that experienced high degrees of alteration, allowing us to obtain a larger collection and reduce extraction biases.
(ii) The late Devonian section at Chanxhe selected for this study may have captured an unusual high abundance of fossil MMs that arrived to Earth following an influx of the ET flux due to an external event (e.g., asteroid break-up, spin-up or tidal disruption of near-Earth objects, arrival of cometary material in the inner Solar System).
(iii) The extraterrestrial spherules recovered from the Chanxhe section show recrystallization of the initial silicate phases to secondary palagonite, an alteration product with a composition that is high in Si and Al and low in Na and K. These local alteration conditions may explain the (relatively) high amount of recovered silicate type CSs (S-types and G-types)
(iv) Lastly, although shallow marine shelf environments are typically oxidizing and not favorable to the preservation of micrometeorites, the late Devonian section at Chanxhe appears to be an exception. The relatively good preservation state of several particles suggests that local depositional conditions—such as low-energy environments, slow sedimentation rates, and geochemical buffering within the carbonate matrix—may have played a role. The Chanxhe limestones contain higher aluminum content, suggesting the presence of fine-grained siliciclastic material that could have further contributed to micrometeorite preservation by limiting oxygen penetration and enhancing early burial.

Origin of the ET flux : triple oxygen isotopic compositions

Triple-oxygen isotope ratios are commonly used to trace the parent body origin of the MMs (e.g. Engrand et al., 1999; Yada et al., 2005; Taylor et al., 2005; Suavet et al., 2010; Cordier and Folco, 2014). Modern CSs have been previously classified into five large isotopic groups (Group 1 to 4 and vestoids) based on their bulk oxygen isotopic values (Fig. 6), taking multiple factors into account : (i) mixing with atmospheric oxygen (presently $\delta^{18}O$ ~23.5‰ and $\delta^{17}O$ ~11.8‰ up to 60.9 km altitude; Thiemens et al., 1995) ; (ii) loss of material by evaporation (Engrand et al., 2005) ; (iii) separation of iron-nickel droplets (Brownlee et al., 1984; Genge and Grady, 1998) which modifies the redox conditions of the remaining melt by removing iron that could otherwise oxidize, thereby altering the oxygen fugacity and promoting the evaporation oxygen-bearing species, leading to mass-dependent oxygen isotope fractionation with higher $\delta^{17}O$ and $\delta^{18}O$ values (Suavet et al., 2010; Fig. 12), and (iv) interaction with terrestrial precipitation forming secondary minerals which can affect the isotopic compositions in the general direction of the water (with an average $\delta^{18}O$ of ~-30‰ for current Antarctica precipitation) (see dashed arrow on Fig. 8). Although Ordovician precipitation near Chanxhe could have a slightly different $\delta^{18}O$, with slightly higher values ~-10‰ (Jones et al., 2020).

Spherules that **plot in proximity of the TFL zone** (75 spherules), with $\Delta^{17}O$ between -0.5 and 0.5 ‰ and positive $\delta^{18}O$ >0.2‰, may derive either from HED or other differentiated asteroids, CI-type material, or enstatite chondrite parent bodies (Fig. 6). Considering their major composition and elemental ratios, their chondritic compositions, quenched textures and droplet morphologies, a fraction of the material is chondritic in nature, implying E-, CI-chondrites or chondritic material that saw extensive exchanges in oxygen following alteration and replacement (Taylor and Brownlee, 1991; Genge et al., 2008, 2016) (Fig. 2-4; Fig. 5; Fig. 8A-F), although the isotopic compositions cannot entirely rule out the terrestrial origin or high terrestrial isotopic overprint of some spherules.

Most particles **distinct from the TFL** plot to the right of the meteorite fields, particularly in the case of S-types, suggesting that similar mechanisms are in play as today in modern MMs, likely involving previously described processes (ii) to (iv) and possibly (i) as well.

A fraction of the I-type particles characterized in this study are plotting away from atmospheric oxygen values (Fig. 6A). High-precision oxygen isotope data for all 22 I-type particles characterized by Fischer et al. (2021) and Pack et al. (2017) showed size range between 400-575 µm, and exhibited $\Delta^{17}O$ values consistent with mesospheric values, as expected when Fe-Ni metal alloys become oxidized during atmospheric entry at altitudes of approximately 80-115 km. Similarly, Engrand et al. (2005) analyzed 11 I-types, all between 400–575 µm in size, though some of their data showed larger uncertainties and some particles showed slight deviations below the TFL.

In this study, a total of 79 CSs, with size ranges between 32-200 µm, are distinguished from atmospheric oxygen, plotting either above (n = 12) or below (n = 67) the TFL, with 12 I-types plotting above, and 23 I-types plotting below the TFL. In general, I-type CSs are plotted more to the left of G-type particles, and even more so than S-type CSs. This trend suggests that progressive oxidation and hydration during terrestrial residence may have shifted their oxygen isotopic composition toward the upper left region, parallel of the TFL. This shift could result from the formation oxyhydroxides, leading to a potential analytical artifact, in which $^{16}OH^-$ is mistakenly detected as $^{17}O^-$, thereby artificially increasing both $\delta^{17}O$ and $\Delta^{17}O$ values (Kita et al., 2009). For instance, the fully replaced and hydrated S-type CS (S4M1B56) plots in this area of the diagram. However, this does not fully explain both the observed $\delta^{18}O$ and large negative deviations in $\Delta^{17}O$ for a subpopulation of the extracted particles.

One key point is that no previous studies have focused specifically on small I-types, as previous studies focus on >400 µm, whereas smaller particles like those analyzed here may undergo incomplete oxidation, leaving inherited isotopic signatures. This hypothesis should be further tested using modern collections of smaller I-types.

Moreover, it is well established that CCs, particularly CM, CO, CR, CI, and C2-ung, contain significant amounts of primary magnetite (up to ~2 wt%), with grain sizes typically <0.1 to 5 µm, and occasionally forming larger framboids or plaquettes (e.g., Sridhar et al., 2021; King et al., 2015; Brearley, 2006). It is therefore plausible that such phases play a more prominent role in smaller I-type spherules. Surprisingly, this effect has not yet been reoirted in modern MM collections, likely due to the limited focus on the smaller size fractions. Further investigation targeting these underexplored size ranges in contemporary collections is needed to confirm this hypothesis.

Identifying the parent bodies of the metallic precursors of I-type spherules is further complicated by the effects of oxidation and evaporation on the composition of individual phases and the effects of evaporation and metal expulsion on the bulk compositions (Genge et al. 2017). The chemical compositions of metal beads in modern I-types, together with consideration of changes in absolute Ni content due to oxidation, suggests that most precursors of such particles derived from CM, CR, H, or iron meteorite kamacite with rare particles derived from taenite (Rudraswami et al., 2014). In the case of the late Devonian I-types analyses here, the triple oxygen isotope signatures preserved are consistent with CM, CR, and ordinary chondrite (OC) parent bodies. Possible explanations include (a) different, smaller sizes preventing effective oxidation, which should be further tested in modern collections, (b) different atmospheric conditions during the late Devonian, or (c) residual interstitial glass in the studied particles. A subset of particles plotting closer to the terrestrial fractionation line (TFL) may represent material from iron meteorites that was oxidized during entry, potentially accounting for up to 37% of the Chanxhe fossil micrometeorite collection.

Micrometeorites that plot **below the TFL values** are commonly linked to bulk carbonaceous chondrites (CCs) (CR, CM, CV, CO) or their refractory inclusions (e.g., Ca-Al-rich inclusions (CAIs)) (Fig. 6). Group 1 and Group 2 carbonaceous CSs are differentiated based on their isotopic compositions, Group 1 CSs have $\Delta^{17}O$ ~-3 to -5‰, and $\delta^{18}O$ in the range of 10-30‰, while Group 2 CSs have $\Delta^{17}O$ ~-1‰, and $\delta^{18}O$ between 15-35‰ (Suavet et al., 2010). The extracted fossil CSs from Chanxhe comprise 10 S-type, 25 G-type, 1 G/I-type, and 23 I-type CSs plotting within or close to the Group 2 and Group 1 fields (Fig. 6). "This observation reinforces the hypothesis of a compositional continuum among spherules derived from various carbonaceous chondrite groups, indicating that the fossil spherules may capture a range of compositions representative of CV, CO, CM, and potentially CR chondrites (Goderis et al., 2020). In addition, 4 S-type (V-type S2M1A51 and CC-type S2M1A66, S2M1A45 and S2M1A46), and 4 G-type (S2M1A3, S2M1A65, S2M1A71, S3M1C15) particles are not linked to any MMs or meteorite group (Fig. 6). Based on their position relative to mixing lines from chondritic fields, they likely originate from chondritic refractory inclusions or other ^{16}O-rich phases found in carbonaceous chondrites (e.g., Genge et al. 1997).

From our extracted spherules, 12 **I-type CSs plot above the TFL** when considering the analytical uncertainty (Fig. 6A). The Group 3 MMs are commonly related to OC, although contributions from enstatite, R or CI chondrites cannot be excluded (Goderis et al. 2020). The Group 4 spherules are characterized by $\delta^{18}O$ above stratospheric oxygen and $\Delta^{17}O$ above 1.0‰ (Fig. 6), and described as ^{16}O-poor spherules in literature (Yada et al., 2005; Suavet et al., 2010). A single I-type particle S2M1B65 with a high $\delta^{18}O$ of 51.25‰ and $\Delta^{17}O$ of 0.45 could be linked to Group 4 (Fig. 6A), similar as the high $\delta^{18}O$ of group 4 observed in Antarctica (Lampe et al., 2022). The origin of these Group 4 spherules remains somewhat uncertain, as this group would need unrealistically high amounts of evaporation to bring the OC or R compositions to those high $\delta^{18}O$ (e.g., Yada et al., 2005; Cordier and Folco, 2014). They have been proposed to derive from fragments of unequilibrated OC, dominated by secondary

magnetite grains ($\Delta^{17}O$ = +5 to +7‰; Choi et al., 1998) or glassy chondrules or feldspathic mesostasis ($\Delta^{17}O$ =+3‰; Franchi et al., 2001). Following the measurement of coexisting ^{16}O-rich and ^{16}O-poor compositions within relict-bearing CSs, a genetic relation of at least some group 4 particles to aqueously altered CCs (i.e., the CM mixing line), with late overprinting of ^{16}O-rich compositions by heavy water has been proposed (Jonker et al. 2024). This is also supported by the observed genetic link between unmelted ^{16}O-poor particles and the CM mixing line as proposed by Suttle et al. (2022). As S2M1B65 spherule is an I-type, composed of magnetite/wüstite, showing an intact metal bead (Fig. 2A), the precursor clearly contained FeNi metal and was already present in the inner Solar System 360 Ma ago.

Of the 160 analyzed CSs (86 I-type, 4 G/I-type, 45 G-type, and 26 S-type particles), 79 fall outside the TFL zone (49.1 %), either above the TFL (in the OC zone) or below the TFL (in the CC zone) (Fig. 6). The 67 spherules (41.6 % of analyzed spherules) in the CC zone include particles from all groups: 4 S-type, 10 S-type, 29 G-type, 1 G/I-type and 23 I-type particles. The 12 CSs in the OC zone (7.5 % of analyzed spherules) are all I-type particles, with a single spherule associated with the ^{16}O-poor reservoir (< 1 % of analyzed spherules). Also, eight of the analyzed spherules plot in the alteration zone (4.3 % of the analyzed spherules), meaning they show too extensive alteration and hydration, and their parent body origin remains unidentified (Table 3). In our extracted spherules, we observed that 47 % of the triple-oxygen analyzed spherules plot close to TFL zone, along the HED origin. Heck et al. (2017) observed that Ordovician ET flux was represented by up to 34 % of achondrites origin, using extracted fossil chromites in marine sediments in northwestern Russia. Indeed, meteorite flux may have varied over geological time, as asteroid family populations could have created variation in the ET flux compositions. Our data do not allow us to conclude on the HED origin of the spherules, but further investigation of the fossil CSs, with trace elements data, could help understand the variation of achondritic flux over time.

In the case of Antarctic MMs, the **ratio of CC to OC** material decreases as the CSs diameter increases, from with a CC/OC ratio of ~ 10 for spherules smaller than 500 µm, compared to a CC/OC ratio of ~ 0.3 for spherules above 500 µm (Goderis et al., 2020). The late Devonian fossil MMs studied here are all small CSs (< 200 µm), which are described to mainly originate from CM and CR chondrites in modern-day collections (Kurat et al., 1994; Brownlee et al., 1997; Engrand and Maurette, 1998; Engrand et al., 2005). Of the particles distinct from the TFL, 15 % derive from OCs and 85 % from CCs, yielding a ratio of CC/OC ratio of ~ 5.6 (Table 3). Indeed, for the I-and G/I-types, 15 % are OC and 30 % are CC related, for a ratio of CC/OC ~ 2. The G- and S-types, 100 % have CC origin (Table 3). The large amount of CC-related MMs compared to meteorites has already been reported in previous collections. Indeed, impact destruction experiments produce dust spherules smaller than 300 µm for hydrous CC targets, compared to OC targets, that produce larger spherules (Flynn et al., 2009). The fossil MMs collected in Chanxhe show more OC-related micrometeorites than more recent micrometeorites collections (e.g. Goderis et al., 2020; Folco and Cordier, 2015). Indeed, only I-types have OCs related origin with a ratio of CCs/OCs in the extracted I-types of 1.9 (Table 3). This can be influenced by : (i) metal grains in OCs are usually larger than in CCs (Genge et al., 2017a); (ii) I-types show larger size range as the S-types and G-types (Fig. 1), and larger size of MMs have higher ratio of OCs compared to CCs; and (iii) I-types compared to S- to G-types show an increase in the oxidation state, pulling all oxygen data toward the hydration zone (see arrow on Fig. 6). The metal- and Fe-oxide-rich petrography of I-type spherules enhances both oxygen incorporation during atmospheric entry and susceptibility to post-depositional alteration. While their oxygen isotope composition mainly reflects interaction with atmospheric oxygen during entry, metal-rich phases can undergo further oxidation after deposition, potentially overprinting the original isotopic signature with a terrestrial signal.

Fossil micrometeorites as a novel proxy for the ET flux

Based on this attempt to reconstruct the past ET flux from late Devonian, most CC parent groups, as well as chondritic refractory inclusions CAIs, and OC parent bodies are represented in fossil CSs. As such, fossil MMs represent an effective proxy to trace the past flux of CC material throughout Earth's history. However, due to the smaller size fraction extracted in fossil MMs, the alteration of larger spherules, and extraction biases, it is possible that the full ET flux might be biased toward CCs. Differences in the composition of the late Devonian atmosphere could also lead to the conservation of a higher proportion of CCs related spherules compared to today's atmosphere, creating the need for a systematic study of fossil micrometeorites across the entire stratigraphic record.

This study shows that the past and present ET flux can be compared, and that fossil MMs represent a valuable proxy to complement existing chemical (e.g., ^{3}He, ^{187}Os/^{188}Os, Ir concentration; Alwmark et al., 2012) and physical (e.g., chromite grains; Schmitz et al. 2019a) to trace the past ET flux. To allow for a detailed comparison with the present day, certain fractions of modern-day collections (e.g., G-type particles) need to be better characterized, and more comprehensive statistical data (e.g. Van Ginneken et al., 2024) should be made available. Despite these current shortcomings, a comparison between the late Devonian fossil MMs and today's MM collections indicates a derivation from comparable parent materials, suggesting that the micrometeorite flux to Earth has sampled similar source material over the last 360 Myr. Fossil micrometeorites also offer the potential to track variations in both relative and absolute abundances, providing insights into the occurrence of specific Solar System events or potential links with Earth's orbital cycles and associated climatic changes. Further investigations of terrestrial preservation conditions, and extraction biases of fossil MMs will aid in further optimizing the use of fossil MMs as an effective proxy to study the past ET flux to Earth.

V. Conclusion

Host rock fragments of carbonates were sampled from a 30-meter stratigraphic interval in the Chanxhe section, Belgium, through the Latest Famennian ~ 360 Myr ago (Becker et al., 2020), before the Devonian-Carboniferous boundary. After dissolution using HCl, 1222 MMs were identified from 26 kg of carbonates through magnetic separation and optical picking from the residue. The majority (90%) were I-type MMs, with G-type particles at 6 %, S-type at 1 %. Additionally, this study describes intermediate G/I-type, constituting < 1 % of the sample, to refine the classification of micrometeorites for fossil collections, based on modern classifications.

Distinguishing ET MMs from terrestrial spherules poses significant challenges, particularly as the geological age of the samples increases weathering in texture and composition. The criteria applied in this study are thought to discriminate identified ET spherules while acknowledging the inherent risk of excluding some altered MMs that closely resemble terrestrial particles. In this study, the Na_2O + K_2O vs Fe/Si ratio plot emerges as a valuable tool for discriminating ET particles. Careful integration of textural and compositional data creates a robust distinction of ET from terrestrial spherules.

The chemical alteration of I-type cosmic spherules, characterized by their quenched dendritic textures and iron-oxidized mineralogy, is marked by significant losses of Ni and Cr, alongside enrichments in Si and Al relative to their modern fresh counterparts. The fossil S-type spherules from Chanxhe exhibit minimal dissolution, with homogeneous weathering of the silicate glass into palagonite. When compared to chondritic values, the compositions of these fossil S-types indicate significant alteration with subchondritic Ni and Mg concentrations. However, some Mg-rich S-types demonstrate a high degree of preservation, making them among the best-preserved S-types in fossil micrometeorite collections. The fossil G-type spherules exhibit patterns that combine characteristics of both I-type and S-type MMs. The preservation of ET chemical signatures, coupled with traces of terrestrial

weathering, in fossil MMs from the late Devonian provides insights into their geological history and contributes additional information to the classification of fossil MMs.

In this study, the spherules are smaller than 125 µm in diameter, compared to modern micrometeorites that peak between 210–330 µm. This smaller size can be explained by the predominance of I- and G-type spherules and the effects of long-term dissolution and weathering of the silicate in marine environments. The Chanxhe S-type spherules presence might be due to extraction methods, a significant influx of ET material during the late Devonian, favorable local alteration processes, and/or ideal sedimentary conditions for preservation.

Using triple oxygen isotopes, among the particles distinct from the TFL, 5.8 % are linked to OCs and 33 % to CCs, resulting in a CC/OC ratio of approximately 5.6. More specifically, about 9% of the I- and G/I-type spherules in the Chanxhe fossil micrometeorite collection are linked to ordinary chondrite (OC) sources, a proportion notably lower than that observed in modern micrometeorite collections, suggesting a higher CC/OC ratio during the studied time interval. Identifying the parent bodies of I-type spherules remains particularly challenging due to the intense oxidation and partial evaporation they experience during atmospheric entry, which alters or erases many original mineralogical and chemical features. Nevertheless, based on the observed geochemical signatures, a portion of I-type spherules are inferred to originate from CC, especially CM and CR groups, or from H-type ordinary chondrites. Fossil MMs from the late Devonian, offer a valuable proxy for tracing ancient ET flux, as they represent various parent body origins. Comparisons to modern MMs collections suggest that the source materials of the ET flux have remained similar over the past 360 Myr. Variations in the ET flux, in both abundance and composition, could bring insights into past Solar System events and changes in Earth's environment, such as oxygen fugacity or CO_2 content. Further research into the preservation and extraction biases of fossil MMs are crucial in order to use the full potential that fossil micrometeorites represent in studying ancient ET flux and paleoenvironmental parameters.

Appendix

Appendix A : Supplementary material

Figure S1 : BSE images of extracted fossil I-type cosmic spherule S1M12A34 interior highlighting the mineralogy, texture and alteration features, showing a corundum inclusion within magnetite.

Figure S2 : BSE images of the interior of extracted fossil G-type cosmic spherule S6M1C66 highlighting the mineralogy and texture with a homogeneous glassy mesostasis and magnetite dendrites.

Table S1. Major elements (oxide xt%) measure by EMPA of the Chanxhe fossil micrometeorites collection.

Table S2. Triple oxygen analyses (SIMS) for the Chanxhe fossil mcirometeorite collection.

Data Availability

Data are available through Zenodo :

https://zenodo.org/records/14547372?preview=1&token=eyJhbGciOiJIUzUxMiJ9.eyJpZCI6IjBkN2QwYzg2LWIxZjktNDBmZS05ODM5LTljNTlhYmJhODMwNSIsImRhdGEiOnt9LCJyYW5kb20iOiI0ZmExMWM0ZjA5Y2M1M2E4YjY0MzFmN2M3NTRiY2Q5NSJ9.vszXyBmfs55VZ5bn2ixCQ5yRauN7bVOnDRIJilTa5yCXLK_zQQ7lxyWgvGzKpYM82GdQ2qHK3wje7lr9_44vbw

Krämer Ruggiu, L., Villeneuve, J., da Silva, A.-C., Debaille, V., Decree, S., Lutz, H., Kaufmann, F., Goderis S. (2025). Supplementary materials and data set for : Diversity among fossil micrometeorites in the late Devonian. Zenodo : https://zenodo.org/records/14547372?preview=1&token=eyJhbGciOiJIUzUxMiJ9.eyJpZCI6IjBkN2QwYzg2LWIxZjktNDBmZS05ODM5LTljNTlhYmJhODMwNSIsImRhdGEiOnt9LCJyYW5kb20iOiI0ZmExMWM0ZjA5Y2M1M2E4YjY0MzFmN2M3NTRiY2Q5NSJ9.vszXyBmfs55VZ5bn2ixCQ5yRauN7bVOnDRIJilTa5yCXLK_zQQ7lxyWgvGzKpYM82GdQ2qHK3wje7lr9_44vbw

Acknowledgement

This research was funded by the European Union through ERC Consolidator Grant FLUX (Tracing the FLUX of cosmic dust arriving to Earth during the Phanerozoic) under grant agreement number 101125231 to SG, as well as the Research Foundation Flanders (FWO) through the FEMINA project number 1295024N to LKR, the Belgian Science Policy Office (BELSPO) through the DESIRED project to SG, VD and SD, and the strategic research fund of the Vrije Universiteit Brussel. LKR thanks the FWO for the funding Postdoctoral Fellowship Junior 1295024N. VD is a Research Director of the Fonds de la Recherche Scientifique FNRS.

CReDIT author statement

LKR: Conceptualization, Data curation, Formal analysis, Funding acquisition (for FWO), Investigation, Methodology, Visualization, Writing – original draft, Writing – review & editing. SG: Conceptualization, Formal analysis, Funding acquisition (for FLUX project), Investigation, Methodology, Supervision, Writing – review & editing. JV: Investigation, Writing – review & editing. ACDS: Investigation, Writing – review & editing. VD: Writing – review & editing, funding acquisition (for DESIRED project). SD: Writing – review & editing funding acquisition (for DESIRED project). LH: Investigation, Writing – review & editing. FEDK: Investigation, Writing – review & editing.

References

Agarwal, D. K., & Palayil, J. K. (2022). Recovery of hydrothermal wustite-magnetite spherules from the Central Indian Ridge, Indian Ocean. *Scientific Reports*, *12*(1), 6811.

Alexander, C. M. D., Taylor, S., Delaney, J. S., Ma, P., & Herzog, G. F. (2002). Mass-dependent fractionation of Mg, Si, and Fe isotopes in five stony cosmic spherules. *Geochimica et Cosmochimica Acta*, *66*(1), 173-183.

Alwmark, C., Schmitz, B., Meier, M. M. M., Baur, H., & Wieler, R. (2012). A global rain of micrometeorites following breakup of the L-chondrite parent body—Evidence from solar wind-implanted Ne in fossil extraterrestrial chromite grains from China. *Meteoritics & Planetary Science*, *47*(8), 1297-1304.

Becker, R. T., Marshall, J. E. A., Da Silva, A. C., Agterberg, F. P., Gradstein, F. M., & Ogg, J. G. (2020). The devonian period. In *Geologic time scale 2020* (pp. 733-810). Elsevier.

Blanchard, M. B., Brownlee, D. E., Bunch, T. E., Hodge, P. W., & Kyte, F. T. (1978). *Meteor ablation spheres from deep-sea sediments* (No. NASA-TM-78510).

Bland W., & Rolls D. (1998). Weathering: an introduction to scientific principles. *Arnold: London*.

Bonté, P., Jehanno, C., Maurette, M., & Brownlee, D. E. (1987). Platinum metals and microstructure in magnetic deep sea cosmic spherules. *Journal of Geophysical Research: Solid Earth*, *92*(B4), E641-E648.

Bottke, W. F., Vokrouhlický, D., Marchi, S., Swindle, T., Scott, E. R. D., Weirich, J. R., & Levison, H. (2015). Dating the Moon-forming impact event with asteroidal meteorites. *Science*, *348*(6232), 321-323.

Brownlee, D. E., Bates, B. A., & Wheelock, M. M. (1984). Extraterrestrial platinum group nuggets in deep-sea sediments. *Nature*, *309*(5970), 693-695.

Brearley, A. J. (2006). The action of water. *Meteorites and the early solar system II*, *943*, 587-624.

Brownlee, D. E., Bates, B., & Schramm, L. (1997). The elemental composition of stony cosmic spherules. *Meteoritics & Planetary Science*, *32*(2), 157.

Choi, B. G., McKeegan, K. D., Krot, A. N., & Wasson, J. T. (1998). Extreme oxygen-isotope compositions in magnetite from unequilibrated ordinary chondrites. *Nature*, *392*(6676), 577-579.

Clayton, R. N., & Mayeda, T. K. (1999). Oxygen isotope studies of carbonaceous chondrites. *Geochimica et Cosmochimica Acta*, *63*(13-14), 2089-2104.

Clayton, R. N., Mayeda, T. K., Goswami, J. N., & Olsen, E. J. (1991). Oxygen isotope studies of ordinary chondrites. *Geochimica et Cosmochimica Acta*, *55*(8), 2317-2337.

Clayton, R. N. (1993). Oxygen isotopes in meteorites. *In: Annual review of earth and planetary sciences. Vol. 21 (A94-10876 01-91), p. 115-149.*, *21*, 115-149.

Cordier, C., & Folco, L. (2014). Oxygen isotopes in cosmic spherules and the composition of the near Earth interplanetary dust complex. *Geochimica et Cosmochimica Acta*, *146*, 18-26.

Cordier, C., Folco, L., Suavet, C., Sonzogni, C., & Rochette, P. (2011). Major, trace element and oxygen isotope study of glass cosmic spherules of chondritic composition: The record of their source material and atmospheric entry heating. *Geochimica et Cosmochimica Acta*, *75*(18), 5203-5218.

Da Silva, A. C., Franck, L., Arts, M., & Denayer, J. (2021). Timing and pacing of the Hangenberg Crisis (Devonian-Carboniferous Boundary) in the Chanxhe sections, Belgium. *Geosciences Made in Belgium*, 186.

Denayer, J., Prestianni, C., Mottequin, B., & Poty, E. (2019). Field trip A1: the uppermost Devonian and Lower Carboniferous in the type area of southern Belgium. In *Kölner Forum für Geologie und Paläontologie* (Vol. 24). Universität zu Köln. Geologisches Institut, Köln, Germany.

Denayer, J., Prestianni, C., Mottequin, B., Hance, L., & Poty, E. (2021). The Devonian–Carboniferous boundary in Belgium and surrounding areas. *Palaeobiodiversity and palaeoenvironments*, *101*(2), 313-356.

Dartois, E., Engrand, C., Brunetto, R., Duprat, J., Pino, T., Quirico, E., Remusat L., Bardin N., Brinani G., Mostefaoui S., Morinaud G., Crane B., Szwec N., Delauche L., Jamme F., Sandt Ch., & Dumas, P. (2013). UltraCarbonaceous Antarctic micrometeorites, probing the Solar System beyond the nitrogen snow-line. *Icarus*, *224*(1), 243-252.

Delvigne, J., Bisdom, E. B. A., Sleeman, J., & Stoops, G. (1979). Olivines, their pseudomorphs and secondary products.

Dredge, I., Parnell, J., Lindgren, P., & Bowden, S. (2010). Elevated flux of cosmic spherules (micrometeorites) in Ordovician rocks of the Durness Group, NW Scotland. *Scottish Journal of Geology*, *46*(1), 7.

Duprat, J., Engrand, C., Maurette, M., Kurat, G., Gounelle, M., & Hammer, C. (2007). Micrometeorites from central Antarctic snow: The CONCORDIA collection. *Advances in Space Research*, *39*(4), 605-611.

Engrand, C., & Maurette, M. (1998). Carbonaceous micrometeorites from Antarctica. *Meteoritics & Planetary Science*, *33*(4), 565-580.

Engrand, C., DeLoule, E., Robert, F., Maurette, M., & Kurat, G. (1999). Extraterrestrial water in micrometeorites and cosmic spherules from Antarctica: An ion microprobe study. *Meteoritics & Planetary Science*, *34*(5), 773-786.

Engrand, C., McKeegan, K. D., Leshin, L. A., Herzog, G. F., Schnabel, C., Nyquist, L. E., & Brownlee, D. E. (2005). Isotopic compositions of oxygen, iron, chromium, and nickel in cosmic spherules: Toward a better comprehension of atmospheric entry heating effects. *Geochimica et Cosmochimica Acta*, *69*(22), 5365-5385.

Fischer, M. B., Oeser, M., Weyer, S., Folco, L., Peters, S. T., Zahnow, F., & Pack, A. (2021). I-Type cosmic spherules as proxy for the Δ′ 17O of the atmosphere—a calibration with quaternary air. *Paleoceanography and Paleoclimatology*, *36*(3), e2020PA004159.

Flynn, G. J., Durda, D. D., Sandel, L. E., Kreft, J. W., & Strait, M. M. (2009). Dust production from the hypervelocity impact disruption of the Murchison hydrous CM2 meteorite: Implications for the disruption of hydrous asteroids and the production of interplanetary dust. *Planetary and Space Science*, *57*(2), 119-126.

Folco, L., Cordier, C. (2015). Micrometeorites. *In Planetary Mineralogy. European MineralogicalUnion*.

Force, E. R., & Cannon, W. F. (1988). Depositional model for shallow-marine manganese deposits around black shale basins. *Economic Geology*, *83*(1), 93-117.

Franchi, I. A., Baker, L., Bridges, J. C., Wright, I. P., & Pillinger, C. T. (2001). Oxygen isotopes and the early Solar System. *Philosophical Transactions of the Royal Society of London. Series A: Mathematical, Physical and Engineering Sciences*, *359*(1787), 2019-2035.

Genge, M. J., & Grady, M. M. (1998). Melted micrometeorites from Antarctic ice with evidence for the separation of immiscible Fe-Ni-S liquids during entry heating. *Meteoritics & Planetary Science*, *33*(3), 425-434.

Genge, M. J., Davies, B., Suttle, M. D., van Ginneken, M., & Tomkins, A. G. (2017a). The mineralogy and petrology of I-type cosmic spherules: Implications for their sources, origins and identification in sedimentary rocks. *Geochimica et Cosmochimica Acta*, *218*, 167-200.

Genge, M. J., Larsen, J., Van Ginneken, M., & Suttle, M. D. (2017b). An urban collection of modern-day large micrometeorites: Evidence for variations in the extraterrestrial dust flux through the Quaternary. *Geology*, *45*(2), 119-122.

Genge, M. J., Engrand, C., Gounelle, M., & Taylor, S. (2008). The classification of micrometeorites. *Meteoritics & Planetary Science*, *43*(3), 497-515.

Genge, M. J., Suttle, M., & Van Ginneken, M. (2016). Olivine settling in cosmic spherules during atmospheric deceleration: An indicator of the orbital eccentricity of interplanetary dust. *Geophysical Research Letters*, *43*(20), 10-646.

Genge, M. J., van Ginneken, M., Suttle, M. D., & Harvey, R. P. (2018). Accumulation mechanisms of micrometeorites in an ancient supraglacial moraine at Larkman Nunatak, Antarctica. *Meteoritics & Planetary Science*, *53*(10), 2051-2066.

Goderis, S., Soens, B., Huber, M. S., McKibbin, S., Van Ginneken, M., Van Maldeghem, F., Debaille V., Greenwood R. C., Franchi I. A., Cnudde V., Van Malderen S., Vanhaecke F., Koeberl C., Topa D., & Claeys, P. (2020). Cosmic spherules from Widerøefjellet, Sør Rondane Mountains (East Antarctica). *Geochimica et Cosmochimica Acta*, *270*, 112-143.

Goderis, S., Sato, H., Ferrière, L., Schmitz, B., Burney, D., Kaskes, P., Vellekoop, J., Wittmann, A., Schultz, T., Chernonozhkin, A. M., Clayes, P., De Graaf, S. J., Déhais, T., De Winter, N. J., Elfman, M., Feignon, J.-G., Ishikawa, A., Koeberl, C., Kristiansson, P., Neal, C. R., Owens, J. D., Schmieder, M., Sinnesael, M., Vanhaecke, F., Van Malderen, A. . M., Bralower, T. J., Gulick, S. P. S., Kring, D. A., KLowery, C. M., Morgan, J. V., Smit, J., Whalen, M. T., & IODP-ICDP Expedition 364 Scientists. (2021). Globally distributed iridium layer preserved within the Chicxulub impact structure. *Science Advances*, *7*(9), eabe3647.

Gooding, J. L. (1986). Clay-mineraloid weathering products in Antarctic meteorites. *Geochimica et Cosmochimica Acta*, *50*(10), 2215-2223.

Goodrich, C. A., & Delaney, J. S. (2000). Fe/Mg–Fe/Mn relations of meteorites and primary heterogeneity of primitive achondrite parent bodies. *Geochimica et Cosmochimica Acta*, *64*(1), 149-160.

Gounelle, M., Chaussidon, M., Morbidelli, A., Barrat, J. A., Engrand, C., Zolensky, M. E., & McKeegan, K. D. (2009). A unique basaltic micrometeorite expands the inventory of solar system planetary crusts. *Proceedings of the National Academy of Sciences*, *106*(17), 6904-6909.

Greenwood, R. C., Schmitz, B., Bridges, J. C., Hutchison, R., & Franchi, I. A. (2007). Disruption of the L chondrite parent body: New oxygen isotope evidence from Ordovician relict chromite grains. *Earth and Planetary Science Letters*, *262*(1-2), 204-213.

Heck, P. R., Schmitz, B., Bottke, W. F., Rout, S. S., Kita, N. T., Cronholm, A., Defouilloy, C., Dronov, A., & Terfelt, F. (2017). Rare meteorites common in the Ordovician period. *Nature Astronomy*, *1*(2), 0035.

Heck, P. R., Ushikubo, T., Schmitz, B., Kita, N. T., Spicuzza, M. J., & Valley, J. W. (2010). A single asteroidal source for extraterrestrial Ordovician chromite grains from Sweden and China: High-precision oxygen three-isotope SIMS analysis. *Geochimica et Cosmochimica Acta*, *74*(2), 497-509.

Heck, P. R., Schmitz, B., Rout, S. S., Tenner, T., Villalon, K., Cronholm, A., Terfelt, F., & Kita, N. T. (2016). A search for H-chondritic chromite grains in sediments that formed immediately after the breakup of the L-chondrite parent body 470 Ma ago. *Geochimica et Cosmochimica Acta*, *177*, 120-129.

Heck, P. R., Schmitz, B., Baur, H., & Wieler, R. (2008). Noble gases in fossil micrometeorites and meteorites from 470 Myr old sediments from southern Sweden, and new evidence for the L-chondrite parent body breakup event. *Meteoritics & Planetary Science*, *43*(3), 517-528.

Hildebrand, A. R., Penfield, G. T., Kring, D. A., Pilkington, M., Camargo Z, A., Jacobsen, S. B., & Boynton, W. V. (1991). Chicxulub crater: a possible Cretaceous/Tertiary boundary impact crater on the Yucatan Peninsula, Mexico. *Geology*, *19*(9), 867-871.

Mathews, J. D., Janches, D., Meisel, D. D., & Zhou, Q. H. (2001). The micrometeoroid mass flux into the upper atmosphere: Arecibo results and a comparison with prior estimates. *Geophysical Research Letters*, *28*(10), 1929-1932.

Jarosewich, E., Nelen, J. A., & Norberg, J. A. (1980). Reference samples for electron microprobe analysis. *Geostandards Newsletter*, *4*(1), 43-47.

Jarosewich, E. (1990). Chemical analyses of meteorites: A compilation of stony and iron meteorite analyses. *Meteoritics*, *25*(4), 323-337.

Jones, D. S., Brothers, R. W., Crüger Ahm, A. S., Slater, N., Higgins, J. A., & Fike, D. A. (2020). Sea level, carbonate mineralogy, and early diagenesis controlled δ13C records in Upper Ordovician carbonates. *Geology*, *48*(2), 194-199.

Jonker, G., van Maldeghem, F., van Ginneken, M., Krämer Ruggiu, L., & Goderis, S. (2024). Oxygen isotopic compositions of fresh rooftop micrometeorites from the Budel collection—Insights into the contemporary cosmic dust flux. *Meteoritics & Planetary Science*.

Kadyrov, R., Glukhov, M., Statsenko, E., & Galliulin, B. (2020). Enigma of ferruginous inclusions in Permian evaporites. *Arabian Journal of Geosciences*, *13*(20), 1058.

King, A. J., Solomon, J. R., Schofield, P. F., & Russell, S. S. (2015). Characterising the CI and CI-like carbonaceous chondrites using thermogravimetric analysis and infrared spectroscopy. *Earth, Planets and Space*, *67*, 1-12.

Kurat, G., Koeberl, C., Presper, T., Brandstätter, F., & Maurette, M. (1994). Petrology and geochemistry of Antarctic micrometeorites. *Geochimica et Cosmochimica Acta*, *58*(18), 3879-3904.

Lampe, S., Soens, B., Chernonozhkin, S. M., de Vega, C. G., van Ginneken, M., Van Maldeghem, F., Vanhaecke, F., Glass, B. P., Franchi, I. A., Terryn, H., Debaille, V., Clayes, P., & Goderis, S. (2022). Decoupling of chemical and isotope fractionation processes during atmospheric heating of micrometeorites. *Geochimica et Cosmochimica Acta*, *324*, 221-239.

Lindskog, A., Costa, M. M., Rasmussen, C. Ø., Connelly, J. N., & Eriksson, M. E. (2017). Refined Ordovician timescale reveals no link between asteroid breakup and biodiversification. *Nature Communications*, *8*(1), 14066.

Love, S. G., & Brownlee, D. E. (1991). Heating and thermal transformation of micrometeoroids entering the Earth's atmosphere. *Icarus*, *89*(1), 26-43.

Meier, M. M. M., Schmitz, B., Baur, H., & Wieler, R. (2010). Noble gases in individual L chondritic micrometeorites preserved in an Ordovician limestone. *Earth and Planetary Science Letters*, *290*(1-2), 54-63.

Morbidelli, A., Lambrechts, M., Jacobson, S., & Bitsch, B. (2015). The great dichotomy of the Solar System: Small terrestrial embryos and massive giant planet cores. *Icarus*, *258*, 418-429.

Murray, J., & Renard, A. F. (1891). *Report on deep-sea deposits based on the specimens collected during the voyage of HMS Challenger in the years 1872 to 1876*. HM Stationery Office.

Murrell, M. T., Davis Jr, P. A., Nishiizumi, K., & Millard Jr, H. T. (1980). Deep-sea spherules from Pacific clay: Mass distribution and influx rate. *Geochimica et Cosmochimica Acta*, *44*(12), 2067-2074.

Mutch, T. A. (1965). Extraterrestrial particles in Paleozoic salts. *Annals of the New York Academy of Sciences, vol. 119, issue 1 Cosmic Dust, pp. 166-185*, *119*, 166-185.

Nelson, D. M., Tréguer, P., Brzezinski, M. A., Leynaert, A., & Quéguiner, B. (1995). Production and dissolution of biogenic silica in the ocean: revised global estimates, comparison with regional data and relationship to biogenic sedimentation. *Global biogeochemical cycles*, *9*(3), 359-372.

NESBITT, H., & WILSON, R. (1992). Department of Geology, University of Western Ontario, London, Ontario, Canada N6A 5B7 ABSTRACT. Relative bulk leach rates of the major elements Na, Ca, Mg, Fe, Al, Ti, and Si from studied basaltic weathering profiles are not. *The American Journal of Science*, *292*(6-10), 740-777.

Newton, J., Franchi, I. A., & Pillinger, C. T. (2000). The oxygen-isotopic record in enstatite meteorites. *Meteoritics & Planetary Science*, *35*(4), 689-698.

Noguchi, T., Ohashi, N., Tsujimoto, S., Mitsunari, T., Bradley, J. P., Nakamura, T., Toh, S., Stephan, T., Iwata, N., & Imae, N. (2015). Cometary dust in Antarctic ice and snow: Past and present chondritic porous micrometeorites preserved on the Earth's surface. *Earth and Planetary Science Letters*, *410*, 1-11.

Onoue, T., Takahata, N., Miura, M., Sato, H., Ishikawa, A., Soda, K., Sano, Y., & Isozaki, Y. (2019). Enhanced flux of extraterrestrial 3 He across the Permian–Triassic boundary. *Progress in Earth and Planetary Science*, *6*, 1-12.

Pack, A., Höweling, A., Hezel, D. C., Stefanak, M. T., Beck, A. K., Peters, S. T., Sengupta, S., Herwartz, D., & Folco, L. (2017). Tracing the oxygen isotope composition of the upper Earth's atmosphere using cosmic spherules. *Nature communications*, *8*(1), 15702.

Prasad, M. S., Rudraswami, N. G., & Panda, D. K. (2013). Micrometeorite flux on Earth during the last~ 50,000 years. *Journal of Geophysical Research: Planets*, *118*(11), 2381-2399.

Reiners, P. W., & Turchyn, A. V. (2018). Extraterrestrial dust, the marine lithologic record, and global biogeochemical cycles. *Geology*, *46*(10), 863-866.

Rubin, A. E. (2018). Carbonaceous and noncarbonaceous iron meteorites: Differences in chemical, physical, and collective properties. *Meteoritics & Planetary Science*, *53*(11), 2357-2371.

Rubin, A. E., & Grossman, J. N. (2010). Meteorite and meteoroid: New comprehensive definitions. *Meteoritics & Planetary Science*, *45*(1), 114-122.

Rudraswami, N. G., Prasad, M. S., Babu, E. V. S. S. K., & Kumar, T. V. (2014). Chemistry and petrology of Fe–Ni beads from different types of cosmic spherules: Implication for precursors. *Geochimica et Cosmochimica Acta*, *145*, 139-158.

Rudraswami, N. G., Pandey, M., Genge, M. J., & Fernandes, D. (2021). Extraterrestrial dust as a source of bioavailable iron contributing to the ocean for driving primary productivity. *Meteoritics & Planetary Science*, *56*(12), 2175-2190.

Sahu, A., Vishwakarma, N., Singh, Y., & Verma, C. B. (2020). Mineral chemistry of high-Al chromian spinel from ultramafic rocks of the Babina–Prithvipur transect, Bundelkhand Craton, central India: Implication for petrogenesis and tectonic setting. *Journal of Earth System Science*, *129*, 1-19.

Savelyev, D. P., Savelyeva, O. L., Moskaleva, S. V., & Rashidov, V. A. (2022). Composition of cosmic spherules from ferromanganese crusts of the Magellan Seamounts. *Geochemistry International*, *60*(5), 411-420.

Schmitz, B., & Häggström, T. (2006). Extraterrestrial chromite in Middle Ordovician marine limestone at Kinnekulle, southern Sweden—Traces of a major asteroid breakup event. *Meteoritics & Planetary Science*, *41*(3), 455-466.

Schmitz, B., Farley, K. A., Goderis, S., Heck, P. R., Bergström, S. M., Boschi, S., Clayes, P., Debaille, V., Dronov, A., Van Ginneken, M., Harper, A. T. D., Iqbal, F., Friberg, J., Liao, S., Martin, E., Meier, M. M. M., Peucker-Ehrenbrink, B., Soens, B., Wieler, R., & Terfelt, F. (2019a). An extraterrestrial trigger for the mid-Ordovician ice age: Dust from the breakup of the L-chondrite parent body. *Science Advances*, *5*(9), eaax4184.

Schmitz, B., Feist, R., Meier, M. M., Martin, E., Heck, P. R., Lenaz, D., Topa, D., Busemann, H., Maden, C., Plant, A. A., & Terfelt, F. (2019b). The micrometeorite flux to Earth during the Frasnian–Famennian transition reconstructed in the Coumiac GSSP section, France. *Earth and Planetary Science Letters*, *522*, 234-243.

Schmitz, B., Lindström, M., Asaro, F., & Tassinari, M. (1996). Geochemistry of meteorite-rich marine limestone strata and fossil meteorites from the lower Ordovician at Kinnekulle, Sweden. *Earth and Planetary Science Letters*, *145*(1-4), 31-48.

Schmitz, B., Peucker-Ehrenbrink, B., Lindström, M., & Tassinari, M. (1997). Accretion rates of meteorites and cosmic dust in the Early Ordovician. *Science*, *278*(5335), 88-90.

Schmitz, B., Tassinari, M., & Peucker-Ehrenbrink, B. (2001). A rain of ordinary chondritic meteorites in the early Ordovician. *Earth and Planetary Science Letters*, *194*(1-2), 1-15.

Schmitz, B., Huss, G. R., Meier, M. M., Peucker-Ehrenbrink, B., Church, R. P., Cronholm, A., Davies, M. B., Heck, P. R., Johanse, A., Keil, K., Kristiansson, P., Ravizza, G., Tassinari, M., & Terfelt, F. (2014).

A fossil winonaite-like meteorite in Ordovician limestone: A piece of the impactor that broke up the L-chondrite parent body?. *Earth and Planetary Science Letters*, *400*, 145-152.

Schulte, P., Alegret, L., Arenillas, I., Arz, J. A., Barton, P. J., Bown, P. R., Bralower, T. J., Christeson, G. L., Claeys, P., Cockell, C.S., Collins, G. S., Deutsch, A., Goldin, T. J., Goto, K., Grajales-Nishimura, J. M., Grieve, R. A. F., Gulick, S. P. S., Johnson, K. R., Kiessling, W., Koeberl, C., Kring, D. A., Macleod, K. G., Matsui, T., Melosh, J., Montanari, A., Morgan, J. V., Neal, C. R., Nichols, D. J., Norris, R. D., Pierazzo, E., Ravizza, G., Rebolledo-Vieyra, M., Reimold, W. U., Robin, E., Salge, T., Speijer, R. P., Sweet, A. R., Urrutia-Fucugauchi, J., Vajda, V., Whalen, M. T., & Willumsen, P. S. (2010). The Chicxulub asteroid impact and mass extinction at the Cretaceous-Paleogene boundary. *Science*, *327*(5970), 1214-1218.

Schulze, H., Bischoff, A., Palme, H., Spettel, B., Dreibus, G., & Otto, J. (1994). Mineralogy and chemistry of Rumuruti: The first meteorite fall of the new R chondrite group. *Meteoritics*, *29*(2), 275-286.

Soens, B., Chernonozhkin, S. M., de Vega, C. G., Vanhaecke, F., Van Ginneken, M., Claeys, P., & Goderis, S. (2022). Characterization of achondritic cosmic spherules from the Widerøefjellet micrometeorite collection (Sør Rondane Mountains, East Antarctica). *Geochimica et Cosmochimica Acta*, *325*, 106-128.

Sridhar, S., Bryson, J. F., King, A. J., & Harrison, R. J. (2021). Constraints on the ice composition of carbonaceous chondrites from their magnetic mineralogy. *Earth and Planetary Science Letters*, *576*, 117243.

Stefánsson, A., & Gíslason, S. R. (2001). Chemical weathering of basalts, Southwest Iceland: effect of rock crystallinity and secondary minerals on chemical fluxes to the ocean. *American Journal of Science*, *301*(6), 513-556.

Suavet, C., Alexandre, A., Franchi, I. A., Gattacceca, J., Sonzogni, C., Greenwood, R. C., Folco, R. C., & Rochette, P. (2010). Identification of the parent bodies of micrometeorites with high-precision oxygen isotope ratios. *Earth and Planetary Science Letters*, *293*(3-4), 313-320.

Suttle, M. D., & Folco, L. (2020). The extraterrestrial dust flux: Size distribution and mass contribution estimates inferred from the Transantarctic Mountains (TAM) micrometeorite collection. *Journal of Geophysical Research: Planets*, *125*(2), e2019JE006241.

Suttle, M. D., & Genge, M. J. (2017). Diagenetically altered fossil micrometeorites suggest cosmic dust is common in the geological record. *Earth and Planetary Science Letters*, *476*, 132-142.

Suttle, M. D., Folco, L., Genge, M. J., Franchi, I. A., Campanale, F., Mugnaioli, E., & Zhao, X. (2021). The aqueous alteration of GEMS-like amorphous silicate in a chondritic micrometeorite by Antarctic water. *Geochimica et Cosmochimica Acta*, *293*, 399-421.

Suttle, M. D., Folco, L., Dionnet, Z., Van Ginneken, M., Di Rocco, T., Pack, A., Scheel, M., & Rotundi, A. (2022). Isotopically heavy micrometeorites—fragments of CY chondrite or a new hydrous parent body?. *Journal of Geophysical Research: Planets*, *127*(8), e2021JE007154.

Suttle, M. D., Campanale, F., Folco, L., Tavazzani, L., Meier, M. M., Miller, C. G., Highes, G., Genge, M. J., Salge, T., Spratt, J., & Anand, M. (2023). Fossil micrometeorites from Monte dei Corvi: Searching for dust from the Veritas asteroid family and the utility of micrometeorites as a palaeoclimate proxy. *Geochimica et Cosmochimica Acta*, *355*, 75-88.

Taylor, S., & Brownlee, D. E. (1991). Cosmic spherules in the geologic record. *Meteoritics*, *26*(3), 203-211.

Taylor, S., Lever, J. H., & Harvey, R. P. (1998). Accretion rate of cosmic spherules measured at the South Pole. *Nature*, *392*(6679), 899-903.

Taylor, S., Lever, J. H., & Harvey, R. P. (2000). Numbers, types, and compositions of an unbiased collection of cosmic spherules. *Meteoritics & Planetary Science*, *35*(4), 651-666.

Taylor, S., Lever, J. H., Harvey, R. P., & Govoni, J. W. (1997). Collecting micrometeorites from the South Pole water well.

Taylor, S., Lever, J. H., & Harvey, R. P. (1998). Accretion rate of cosmic spherules measured at the South Pole. *Nature*, *392*(6679), 899-903.

Taylor, S., Delaney, J., Ma, P., Herzog, G. F., & Engrand, C. (2005). Isotopic fractionation of iron, potassium, and oxygen in stony cosmic spherules: Implications for heating histories and sources. *Geochimica et Cosmochimica Acta*, *69*(10), 2647-2662.

Terfelt, F., & Schmitz, B. (2021). Asteroid break-ups and meteorite delivery to Earth the past 500 million years. *Proceedings of the National Academy of Sciences*, *118*(24), e2020977118.

Thiemens, M. H., Jackson, T. L., & Brenninkmeijer, C. A. (1995). Observation of a mass independent oxygen isotopic composition in terrestrial stratospheric CO2, the link to ozone chemistry, and the possible occurrence in the Martian atmosphere. *Geophysical Research Letters*, *22*(3), 255-257.

Tomkins, A. G., Bowlt, L., Genge, M., Wilson, S., Brand, H. E., & Wykes, J. L. (2016). Ancient micrometeorites suggestive of an oxygen-rich Archaean upper atmosphere. *Nature*, *533*(7602), 235-238.

Toppani, A., Libourel, G., Engrand, C., & Maurette, M. (2001). Experimental simulation of atmospheric entry of micrometeorites. *Meteoritics & Planetary Science*, *36*(10), 1377-1396.

Van Ginneken, M., Wozniakiewicz, P. J., Brownlee, D. E., Debaille, V., Della Corte, V., Delauche, L., Duprat J., Engrand, C., Folco, L., Fries, M., Gattacceca, J., Genge, M. J., Goderis, S., Gounelle, M., Harvey, R. P., Jonker, G., Krämer Ruggiu, L., Larsen, J., Lever, J. H., Noguchi, T., Peterson, S., Rochette, P., Rojas, J., Rotundi, A., Rudraswami, G., G., Suttle, M. D., Taylor, S., Van Maldeghem, F., & Zolensky, M. (2024). Micrometeorite collections: a review and their current status. *Philosophical Transactions A*, *382*(2273), 20230195.

Van Ginneken, M., Genge, M. J., Folco, L., & Harvey, R. P. (2016). The weathering of micrometeorites from the Transantarctic Mountains. *Geochimica et Cosmochimica Acta*, *179*, 1-31.

Van Maldeghem, F., Van Ginneken, M., Soens, B., Kaufmann, F., Lampe, S., Krämer Ruggiu, L., Hecht, L., Clayes, P., & Goderis, S. (2023). Geochemical characterization of scoriaceous and unmelted micrometeorites from the Sør Rondane Mountains, East Antarctica: Links to chondritic parent bodies and the effects of alteration. *Geochimica et Cosmochimica Acta*, *354*, 88-108.

Voldman, G. G., Genge, M. J., Albanesi, G. L., Barnes, C. R., & Ortega, G. (2013). Cosmic spherules from the Ordovician of Argentina. *Geological Journal*, *48*(2-3), 222-235.

Yada, T., Nakamura, T., Noguchi, T., Matsumoto, N., Kusakabe, M., Hiyagon, H., Ushikuo, T., Sugiura, N., Kojima, H., & Takaoka, N. (2005). Oxygen isotopic and chemical compositions of cosmic spherules collected from the Antarctic ice sheet: Implications for their precursor materials. *Geochimica et Cosmochimica Acta*, *69*(24), 5789-5804.

Zolensky, M., Bland, P., Brown, P., & Halliday, I. (2006). Flux of extraterrestrial materials. *Meteorites and the early solar system II*, *943*, 869-888.

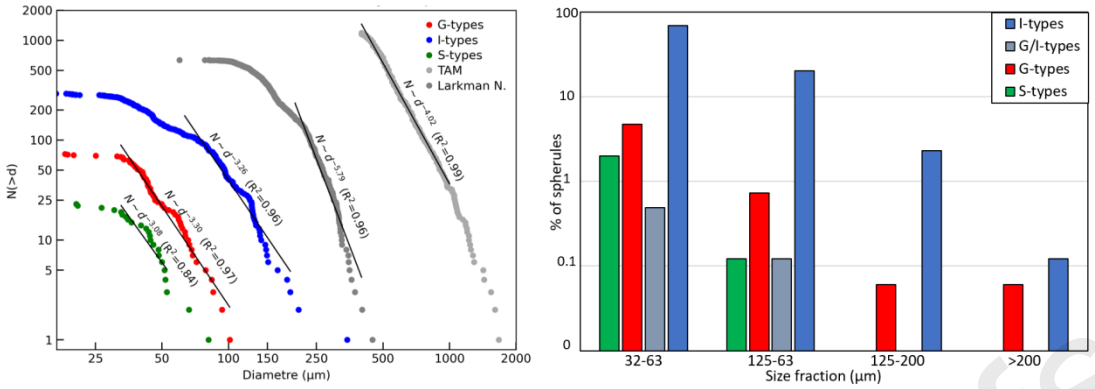

Figure 1 : (Left) Cumulative size distribution for late Devonian fossil cosmic spherules by types, compared to Antarctic collection from the Transantarctic Mountains (>400 µm size fraction), and Larkman nunatak (>60 µm) (Genge et al., 2018; and Suavet et al., 2009). The slopes are calculated for : >63 µm for S-types; 32-125 µm for G-types; 63-200 µm for I-types; 200-400 µm for Larkman N.; and 400-1000 µm for TAM. (Right) Comparison of size distribution for the 1222 cosmic spherules extracted from the late Devonian carbonates sampled at the Chanxhe section, Liège, Belgium.

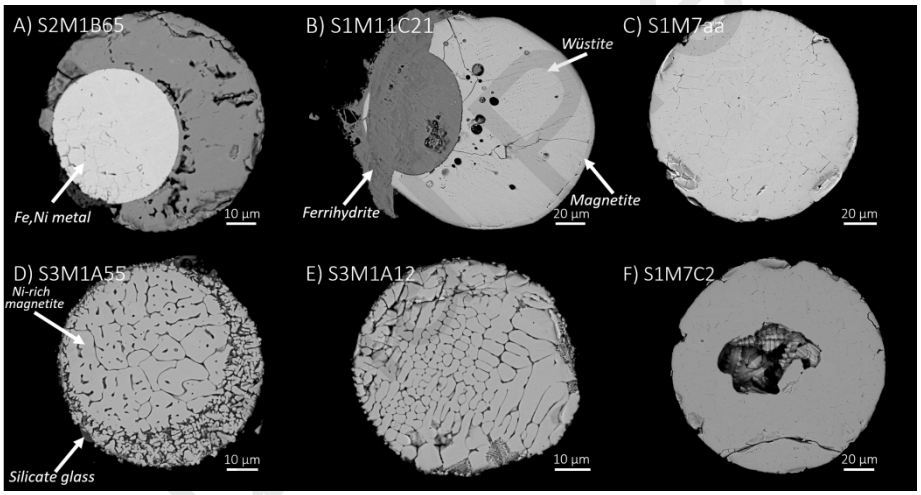

Figure 2 : BSE images of extracted fossil I-type and G/I-type cosmic spherule interiors highlighting their mineralogy, texture and alteration features. A) I-type cosmic spherule showing a preserved metal bead; B) I-type cosmic spherule with a metal inclusion altered into ferrihydrite; C) Typical OX I-type cosmic spherule composed of magnetite; D) G/I-type cosmic spherule showing an inner part that is I-type-like and enriched in Ni and an outer rim part that is G-type-like; E) G/I-type cosmic spherule ; F) Typical MET I-type cosmic spherule composed of wüstite and magnetite.

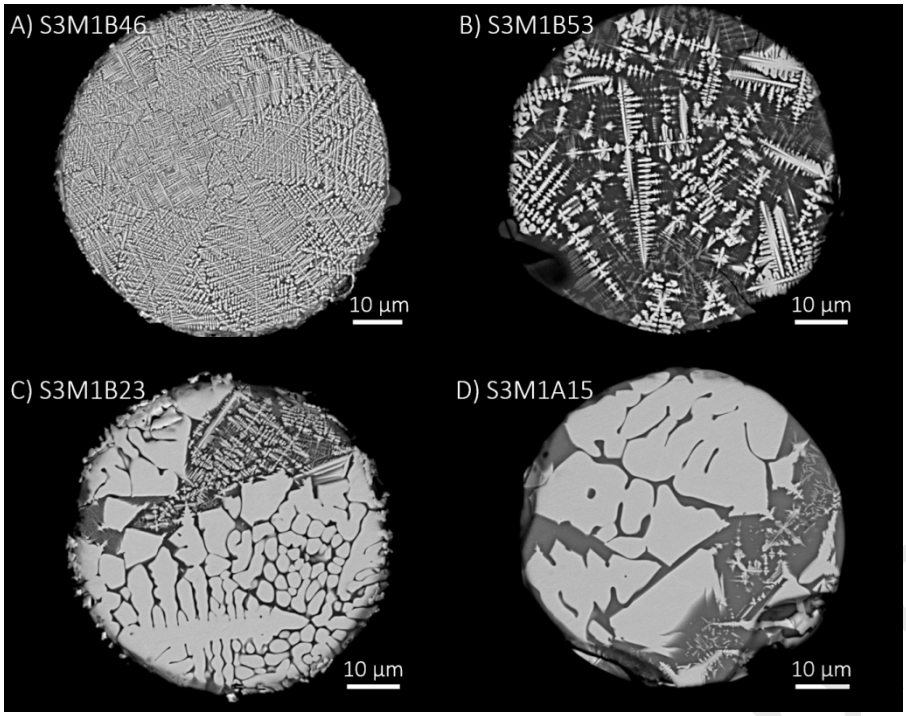

Figure 3 : BSE images of extracted fossil G-type cosmic spherule interiors highlighting their mineralogy, texture and alteration features. A-D) G-types spherules with textures changing from fine to bulky magnetite.

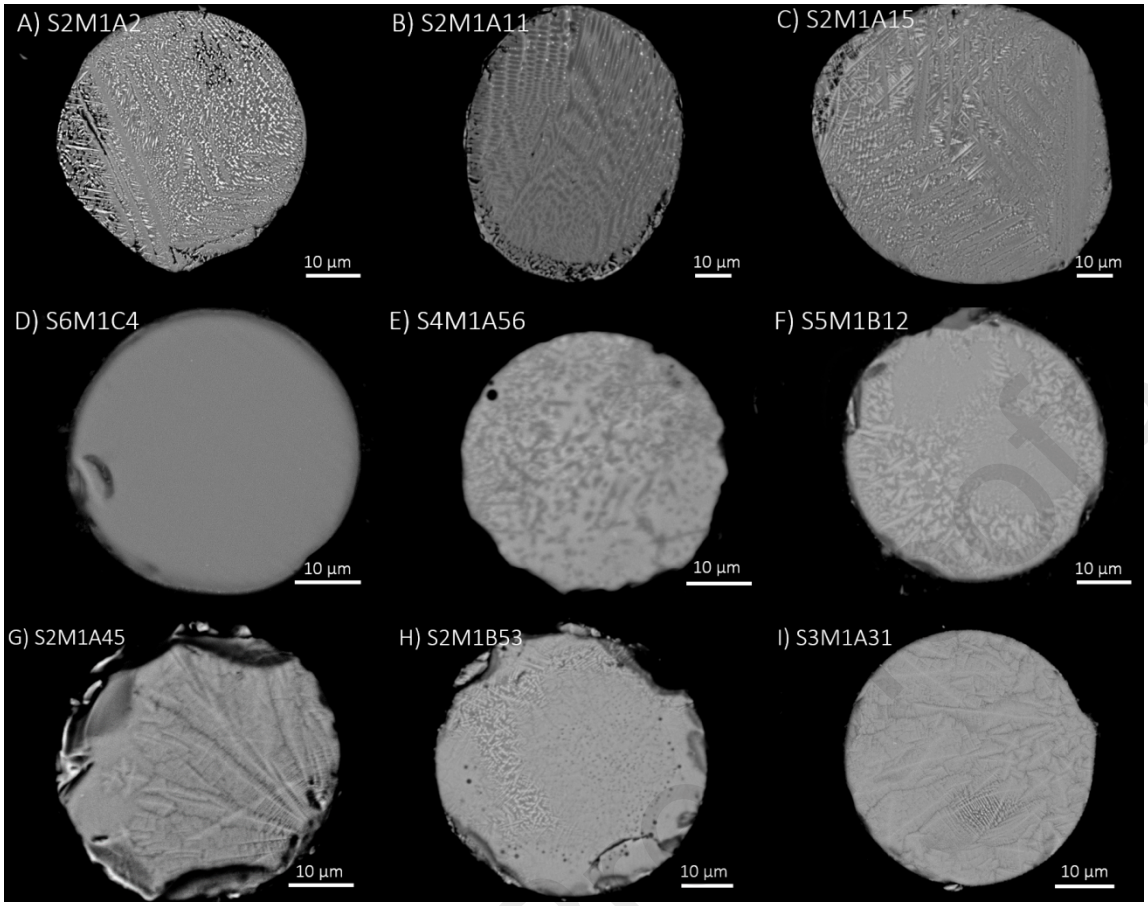

Figure 4 : BSE images of extracted fossil S-type cosmic spherule interiors highlighting their mineralogy, texture and alteration features. A-C) Mg-rich S-type cosmic spherules retaining their BO texture; D-I) Mg-poor S-type cosmic spherule with V-type (D), PO-type (E) and CC-type (F-I) textures.

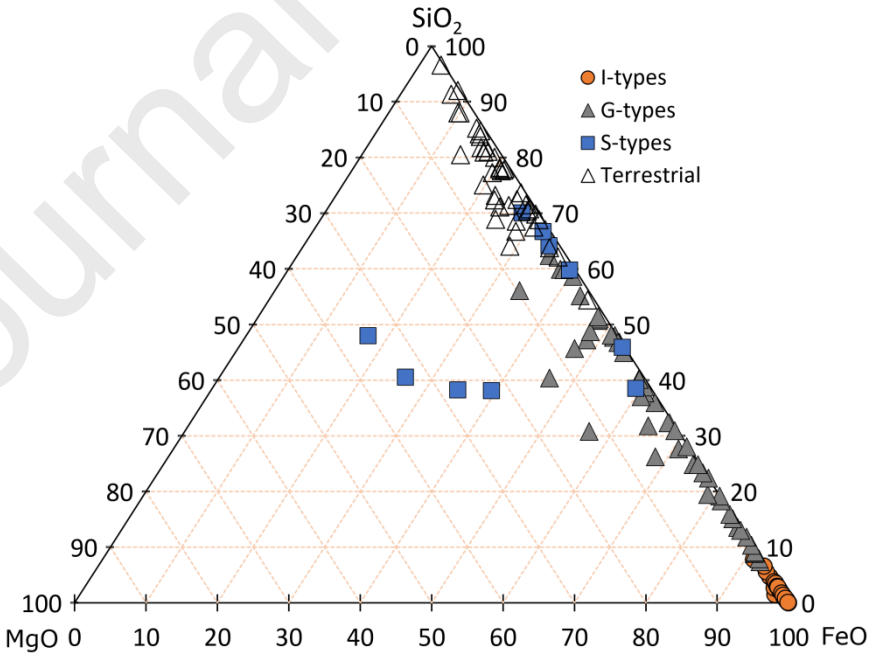

Figure 5 : Ternary atomic Mg-Si-Fe presenting EMPA data for the extracted fossil CSs subdivided into S-type, G-type and I-type cosmic spherules, compared to other terrestrial spherules recovered from the same sediments.

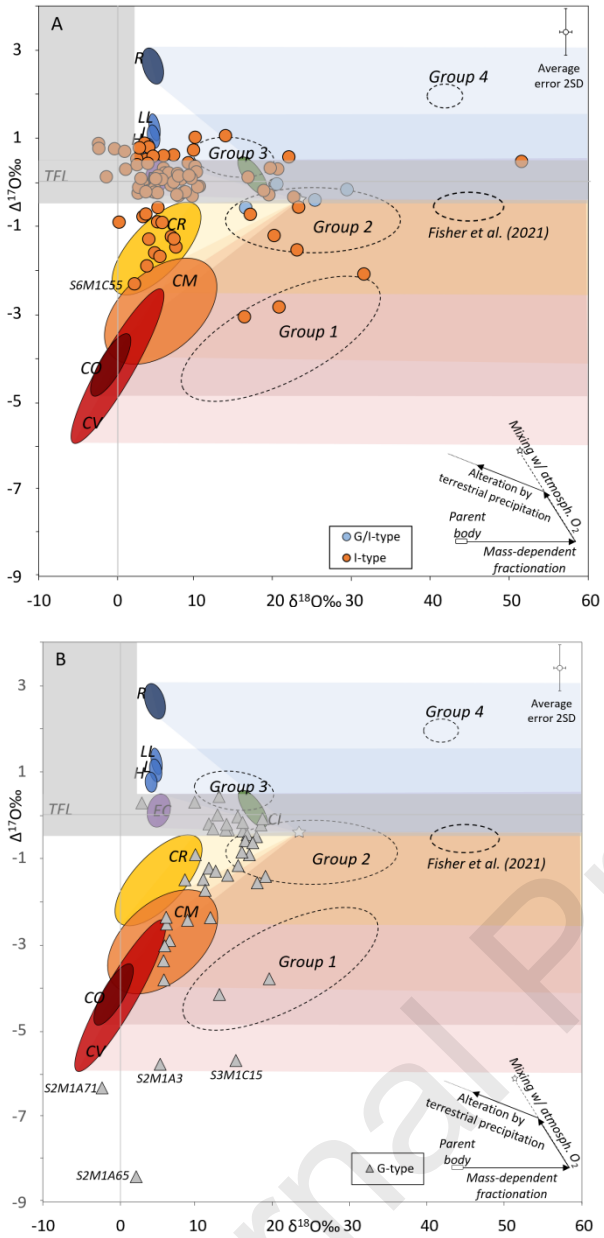

Figure 6 : Triple oxygen data by SIMS for the extracted fossil cosmic spherules represented in a plot of $\delta^{18}O$ (horizontal) versus $\Delta^{17}O$ (vertical) in ‰. The solid line represents the terrestrial fractionation line TFL (~ $\delta^{17}O = 0.52 \times \delta^{18}O$). The star represents the present average isotopic composition of oxygen around the transition from the stratosphere to the mesosphere ($\delta^{18}O$ ~ 23.5‰ and $\delta^{17}O$ ~ 11.8‰; Thiemens et al., 1995). The plots are adapted from Suavet et al. (2010) and Cordier and Folco (2014): colored domains represent potential meteoritical parent bodies (Clayton et al., 1991; Schulze et al., 1994; Clayton and Mayeda, 1999; Newton et al., 2000), while color-shaded areas designate the range of possible values for MMs derived from the particular parent body. The outlines of the 4 groups originally identified by Suavet et al. (2010), and a group from Fisher et al. (2021) particles are represented using dotted lines. Dashed arrows reflect the direction of possible shifts due to the atmospheric entry and formation of alteration products in equilibrium with terrestrial precipitation. Analytical uncertainties for SIMS measurements are ± 0.4 ‰ for $\delta^{18}O$ and ± 0.5‰ for $\Delta^{17}O$ (2σ). With standard deviation being on average $\delta^{18}O$ ± 0.4 ‰ and $\Delta^{17}O$ ± 0.5 ‰, grey zones represent data that may have experienced extensive hydration from terrestrial precipitation (positive $\Delta^{17}O$ and $\delta^{18}O$ < 0.2‰) and potential TFL overprints ($\Delta^{17}O$ between -0.5 and 0.5‰). (A) I-type and G/I-type, (B) G-type cosmic spherules and (C) S-types.

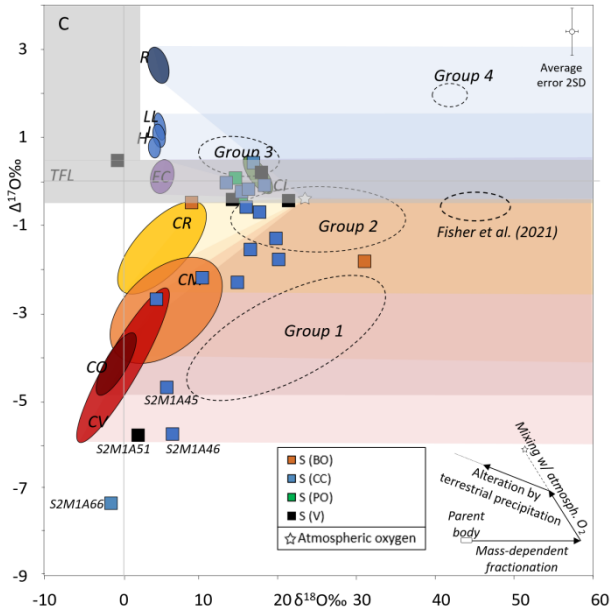

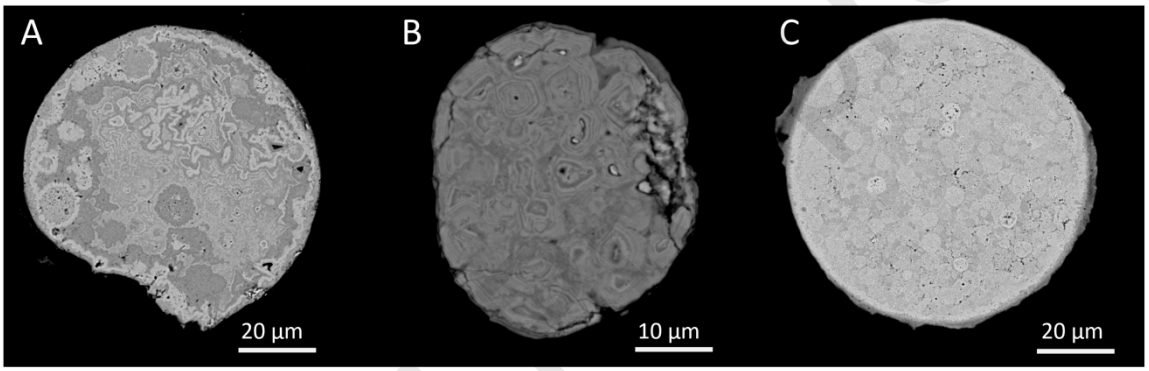

Figure 7 : BSE images of representative other particles extracted from the sediments, with no indications of ET nature. A) A spherule composed of layered magnetite and hematite; B) Layered magnetite; C) Fe-sulphide spherules with a framboidal texture in combination with magnetite.

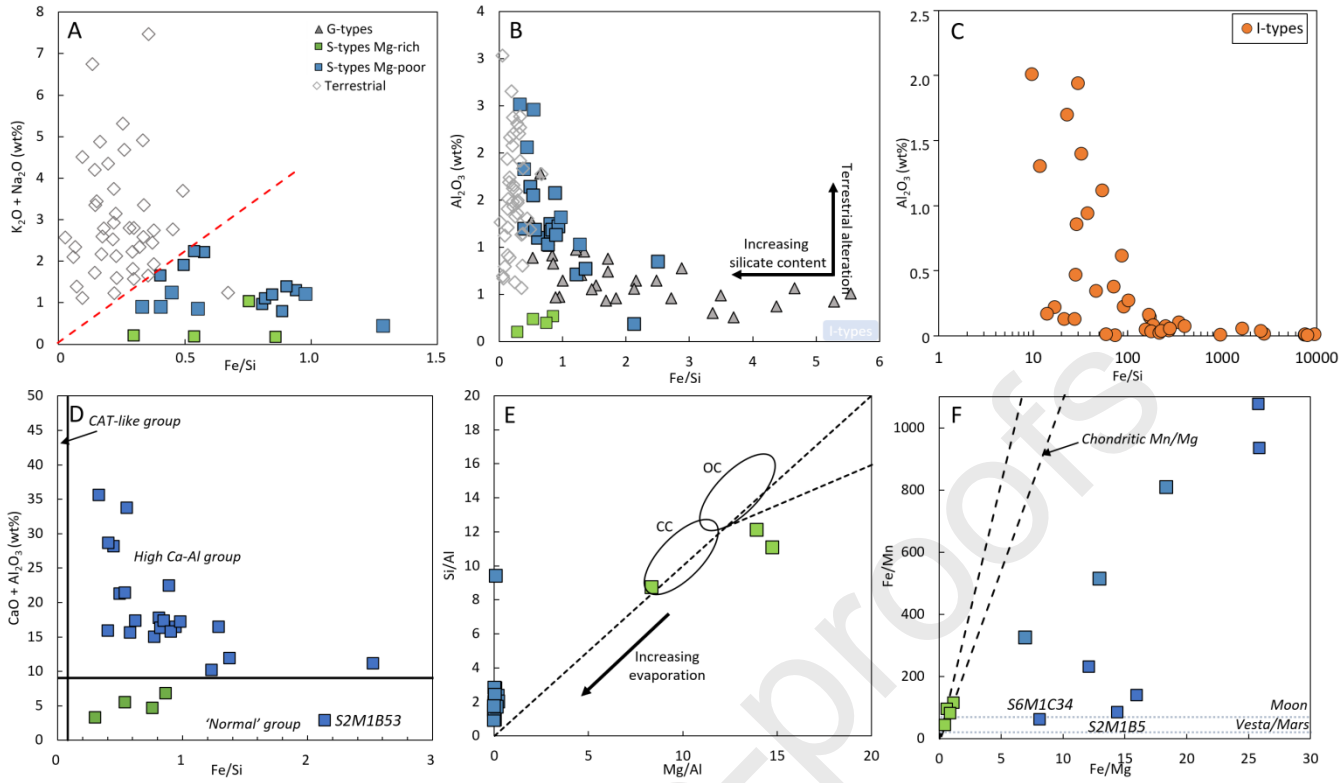

Figure 8 : Major elements diagrams for extracted late Devonian fossil micrometeorites. A) Fe/Si (atomic) vs K_2O+Na_2O (wt%) allowing to distinguish terrestrial and extraterrestrial spherules. B-C) Fe/Si (atomic) vs Al_2O_3 (wt%) enabling to distinguish different CSs type cosmic spherules and increasing terrestrial alteration trends for S-types, G-types (G- + G/I-types) (B), and I-types (C). D) Fe/Si (atomic) vs CaO + Al_2O_3 (wt%). The definition for the three groups of chondritic S-type CSs are based on estimates by Taylor et al. (2000) and Cordier et al. (2011). E) Mg/Al vs Si/Al (atomic), showing the evaporation trajectory from the Ivuna-type (CI) carbonaceous chondrite precursor (fields from Jarosewich, 1990). Regardless of the starting composition, evaporation trajectories for carbonaceous and ordinary chondritic compositions converge after ~30% of the material has evaporated (Alexander et al., 2002) (CC = carbonaceous chondrite field; OC = ordinary chondrite field). F) Fe/Mg vs Fe/Mn (atomic). Chondrites and achondrites fields are based on Goodrich and Delaney (2000).

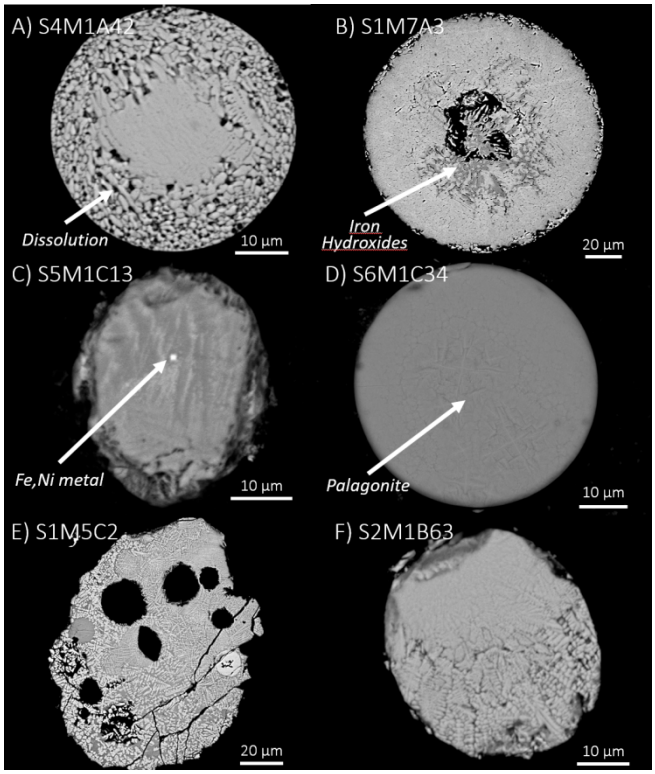

Figure 9 : BSE images of weathered spherules. A–B: I-type spherules exhibiting edge dissolution (A) and interior oxidation into ferrihydrite (B). C–D: S-type spherules showing extensive edge dissolution (C) and complete recrystallization into palagonite (D). E–F: G-type spherules with significant dissolution of the silicate portions

Table 1
Average Major (oxide wt%) element composition with standard deviation (SD; italic) of textural and chemical groups of extracted G-type, G/I-type and I-type fossil cosmic spherules, determined by electron microprobe analysis (EMPA).

	I-types (n=43)				G/I-types (n=7)				G-types (n=33)			
	Average	Min	Max	*SD*	Average	Min	Max	*SD*	Average	Min	Max	*SD*
SiO_2 (wt%)	1.24	bdl	6.53	1.58	7.91	6.18	10.5	1.37	65.0	10.9	41.8	9.01
TiO_2	0.03	bdl	0.15	0.04	0.16	bdl	0.58	0.18	0.72	0.02	3.10	0.65
Al_2O_3	0.36	bdl	2.01	0.55	1.44	bdl	3.19	1.06	9.39	3.20	22.95	4.29
Cr_2O_3	0.31	bdl	4.07	0.69	0.01	bdl	0.02	0.00	0.02	bdl	0.14	0.02
FeO	86.2	68.6	97.6	4.71	77.7	72.0	81.5	2.80	48.4	19.0	72.6	15.1
MnO	0.47	bdl	2.79	0.61	0.08	bdl	0.37	0.13	0.32	bdl	3.01	0.71
MgO	0.09	bdl	0.92	0.19	0.14	bdl	0.32	0.10	1.72	0.02	9.83	2.58
CaO	0.23	bdl	3.12	0.56	0.68	0.01	2.11	0.77	2.04	0.07	7.78	1.97
P_2O_5	0.07	bdl	0.61	0.12	0.11	0.01	0.43	0.14	0.21	0.04	0.91	0.19
SO_3	0.05	bdl	0.69	0.15	0.01	bdl	0.03	0.01	<0.01	bdl	0.04	0.01
Cl	0.01	bdl	0.06	0.01	0.02	bdl	0.05	0.02	0.02	bdl	0.10	0.02
NiO	0.12	bdl	3.73	0.56	0.09	0.01	0.41	0.13	0.02	bdl	0.08	0.02
ZnO	0.03	bdl	0.12	0.03	0.02	bdl	0.04	0.01	0.03	bdl	0.10	0.02
V_2O_3	0.04	bdl	0.84	0.12	0.03	0.01	0.06	0.02	0.11	0.01	0.98	0.17
Total	89.3	73.3	100	3.8	88.4	82.7	90.4	2.44	89.0	69.0	94.7	4.63
Fe/Si (atomic)	3352	9.77	73988	*11427*	8.43	6.26	10.37	*1.29*	2.01	0.47	5.57	*1.42*
Fe/Mg	10989	48.8	148733	*25021*	3702	137	1762	*7536*	140	1.96	1762	*325*
Fe/Mn	2338	bdl	18316	*4242*	44986	2099	233702	*49504*	5997	18.16	105009	*18171*
Mg/Al	0.39	bdl	6.87	*1.03*	1.64	0.05	10.64	*3.67*	0.29	Bdl	2.26	*0.49*
Mg/Si	0.31	bdl	4.97	*0.87*	0.03	bdl	0.06	*0.02*	0.09	bdl	0.61	*0.14*

n= number of spherules measured. Bdl : below detection limit.

Table 2
Average Major (oxide wt%) element composition with standard deviation (SD; italic) of textural and chemical groups of extracted different S-types fossil cosmic spherules compared to terrestrial extracted spherules. Determined by electron microprobe analysis (EMPA).

	S-types all (n=26)				S-types Mg-rich (n=4)				S-types Mg-poor (n=22)				Terrestrial (n=42)			
	Average	Min	Max	*SD*	Average	Min	Max	*SD*	Average	Min	Max	*SD*	Average	Min	Max	*SD*
SiO_2 (wt%)	36.6	20.1	51.6	*6.78*	37.6	34.0	43.7	*3.87*	36.7	20.1	51.6	*7.18*	53.2	9.25	77.7	*11.6*
TiO_2	0.60	0.03	1.78	*0.49*	0.13	0.10	0.16	*0.02*	0.69	0.03	1.78	*0.42*	0.67	0.09	1.81	*0.46*
Al_2O_3	14.7	1.23	32.4	*8.20*	2.51	1.23	3.36	*0.80*	16.9	2.33	32.4	*6.89*	19.38	4.56	39.0	*7.79*
Cr_2O_3	0.06	bdl	0.43	*0.11*	0.29	0.09	0.43	*0.13*	0.02	bdl	0.04	*0.01*	0.02	bdl	0.14	*0.03*
FeO	34.0	15.4	64.7	*11.6*	26.6	15.6	35.0	*7.39*	35.4	15.4	64.7	*11.6*	14.7	2.29	31.2	*6.71*
MnO	0.18	bdl	0.63	*0.19*	0.35	0.27	0.41	*0.06*	0.13	bdl	0.63	*0.18*	0.14	bdl	2.35	*0.34*
MgO	4.82	0.18	31.8	*9.63*	27.0	20.0	31.8	*4.91*	0.80	0.18	2.51	*0.54*	1.58	0.13	5.29	*1.37*
CaO	1.81	0.19	5.21	*1.19*	2.53	2.04	3.42	*0.54*	1.68	0.19	5.21	*1.23*	1.56	0.20	7.65	*1.57*
P_2O_5	0.35	0.02	1.32	*0.28*	0.11	0.02	0.24	*0.08*	0.40	0.10	1.32	*0.28*	0.27	0.02	1.93	*0.42*
NiO	0.15	bdl	1.62	*0.39*	0.89	0.03	1.62	*0.57*	0.02	bdl	0.07	*0.01*	0.02	bdl	0.08	*0.02*
ZnO	0.02	bdl	0.07	*0.02*	0.01	bdl	0.02	*0.01*	0.02	bdl	0.07	*0.01*	0.01	bdl	0.06	*0.02*
Na_2O	0.28	0.01	0.83	*0.24*	0.22	0.01	0.83	*0.35*	0.29	bdl	0.73	*0.02*	0.72	0.09	3.01	*0.62*
K_2O	0.66	bdl	1.58	*0.47*	0.02	bdl	0.05	*0.02*	0.83	0.03	1.58	*0.38*	2.26	0.63	7.32	*1.49*
Total	94.1	85.4	100	*4.32*	98.2	96.2	100	*1.40*	93.3	85.4	100	*4.25*	93.3	2.50	98.8	*13.8*
Fe/Si (atomic)	0.86	0.30	2.52	*0.51*	0.61	0.30	0.86	*0.22*	0.90	0.33	2.52	*0.53*	0.25	0.03	0.67	*0.13*
Fe/Mg	35.7	0.27	186	*46.5*	0.60	0.27	0.98	*0.27*	43.3	6.80	186	*47.7*	10.3	1.37	56.1	*10.6*
Fe/Mn	804	38.0	4258	*1064*	78.5	38.0	110	*26.3*	1057	56.0	4258	*1126*	605	8.62	4242	*927*
Mg/Al	1.30	0.01	16.4	*3.52*	18.4	8.38	36.4	*10.7*	0.11	0.01	0.11	*0.03*	0.14	bdl	0.74	*0.16*
Mg/Si	0.19	0.01	1.23	*0.38*	1.06	0.88	1.23	*0.12*	0.10	0.01	0.10	*0.03*	0.04	bdl	0.16	*0.04*
$Al_2O_3+K_2O$ (w%)	15.2	1.23	33.1	*8.49*	2.53	1.23	3.36	*0.80*	33.1	2.33	33.1	*7.11*	22.2	9.40	40.4	*7.51*
K_2O+Na_2O	0.94	0.01	2.10	*0.59*	0.24	0.01	0.88	*0.37*	1.12	0.27	2.10	*0.50*	2.87	0.96	7.41	*1.43*

n= number of spherules measured. Bdl : below detection limit.

Table 3
Distribution of textural group of the 161 extracted fossil CSs analyzed for triple oxygen isotopic composition, and related percentage statistics for parent body origin.

Textural group	Number of analyzed spherules	*%*	OC related	*%*	CC related	*%*	Overlap with TFL (incl. CI, EC, HED)	*%*	Hydration zone (unidentified)	*%*
I-type	87	*54*	12	*100*	23	*34*	46	*62*	6	*75*
G/I-type	4	*2.5*	0	*0*	1	*1.5*	3	*4.0*	0	*0*
G-type	43	*28*	0	*0*	28	*41*	15	*20*	0	*0*
S-type	26	*17*	0	*0*	15	*22*	10	*14*	2	*25*
Total	160	*100*	12	*100*	67	*100*	74	*100*	8	*100*

Table 1

Average Major (oxide wt%) element composition with standard deviation (SD; italic) of textural and chemical groups of extracted G-type, G/I-type and I--type fossil cosmic spherules, determined by electron microprobe analysis (EMPA).

	I-types (n=43)					G/I-types (n=7)					G-types (n=33)				
	Average	Min	Max	*SD*		Average	Min	Max	*SD*		Average	Min	Max	*SD*	
SiO_2 (wt%)	1.24	bdl	6.53	1.58		7.91	6.18	10.5	1.37		65	10.9	41.8	9.01	
TiO_2	0.03	bdl	0.15	0.04		0.16	bdl	0.58	0.18		0.72	0.02	3.1	0.65	
Al_2O_3	0.36	bdl	2.01	0.55		1.44	bdl	3.19	1.06		9.39	3.2	22.95	4.29	
Cr_2O_3	0.31	bdl	4.07	0.69		0.01	bdl	0.02	0		0.02	bdl	0.14	0.02	
FeO	86.2	68.6	97.6	4.71		77.7	72	81.5	2.8		48.4	19	72.6	15.1	
MnO	0.47	bdl	2.79	0.61		0.08	bdl	0.37	0.13		0.32	bdl	3.01	0.71	
MgO	0.09	bdl	0.92	0.19		0.14	bdl	0.32	0.1		1.72	0.02	9.83	2.58	
CaO	0.23	bdl	3.12	0.56		0.68	0.01	2.11	0.77		2.04	0.07	7.78	1.97	
P_2O_5	0.07	bdl	0.61	0.12		0.11	0.01	0.43	0.14		0.21	0.04	0.91	0.19	

SO_3	0.05	bdl	0.69	0.15		0.01	bdl	0.03	0.01		<0.01	bdl	0.04	0.01	
Cl	0.01	bdl	0.06	0.01		0.02	bdl	0.05	0.02		0.02	bdl	0.1	0.02	
NiO	0.12	bdl	3.73	0.56		0.09	0.01	0.41	0.13		0.02	bdl	0.08	0.02	
ZnO	0.03	bdl	0.12	0.03		0.02	bdl	0.04	0.01		0.03	bdl	0.1	0.02	
V_2O_3	0.04	bdl	0.84	0.12		0.03	0.01	0.06	0.02		0.11	0.01	0.98	0.17	
Total	89.3	73.3	100	3.8		88.4	82.7	90.4	2.44		89	69	94.7	4.63	
Fe/Si (atomic)	3352	9.77	73988	*11427*		8.43	6.26	10.37	*1.29*		2.01	0.47	5.57	*1.42*	
Fe/Mg	10989	48.8	148733	*25021*		3702	137	1762	*7536*		140	1.96	1762	*325*	
Fe/Mn	2338	bdl	18316	*4242*		44986	2099	233702	*49504*		5997	18.16	105009	*18171*	
Mg/Al	0.39	bdl	6.87	*1.03*		1.64	0.05	10.64	*3.67*		0.29	Bdl	2.26	*0.49*	
Mg/Si	0.31	bdl	4.97	*0.87*		0.03	bdl	0.06	*0.02*		0.09	bdl	0.61	*0.14*	
n= number of spherules measured. Bdl : below detection limit.															

Table 2

Average Major (oxide wt%) element composition with standard deviation (SD; italic) of textural and chemical groups of extracted different S-types fossil cosmic spherules compared to terrestrial extracted spherules. Determined by electron microprobe analysis (EMPA).

	S-types all (n=26)				S-types Mg-rich (n=4)				S-types Mg-poor (n=22)				Terrestrial (n=42)			
	Average	Min	Max	*SD*	Average	Min	Max	*SD*	Average	Min	Max	*SD*	Average	Min	Max	*SD*
SiO_2 (wt%)	36.6	20.1	51.6	*6.78*	37.6	34	43.7	*3.8 7*	36.7	0.1	51.6	*7.18*	53.2	9.25	77.7	*1.16*
TiO_2	0.6	0.03	1.78	*0.49*	0.13	0.1	0.16	*0.02*	0.69	0.03	1.78	*0.42*	0.67	0.09	1.81	*0.46*
Al_2O_3	14.7	1.23	32.4	*8.2*	2.51	2.13	3.6	*0.8*	16.9	3.3	32.4	*6.89*	19.38	4.56	39	*7.79*
Cr_2O_3	0.06	bdl	0.43	*0.11*	0.29	0.09	0.43	*0.13*	0.02	bdl	0.04	*0.01*	0.02	bdl	0.14	*0.03*
FeO	34	15.4	64.7	*11.6*	26.6	15.6	35	*7.39*	35.4	15.4	64.7	*11.6*	14.7	2.29	31.2	*6.71*
MnO	0.18	bdl	0.63	*0.19*	0.35	0.27	0.41	*0.06*	0.13	bdl	0.63	*0.18*	0.14	bdl	2.35	*0.34*
MgO	4.82	0.18	31.8	*9.63*	27	20	31.8	*4.91*	0.8	0.18	2.51	*0.54*	1.58	0.13	5.29	*1.37*

	1.81	0.19	5.21	*1.19*	2.53	2.04	3.42	*0.54*	1.68	0.19	5.21	*1.23*	1.56	0.02	7.65	*1.57*
CaO																
	0.35	0.02	1.32	*0.28*	0.11	0.02	0.24	*0.08*	0.41	0.01	1.32	*0.28*	0.27	0.02	1.93	*0.42*
P_2O_5																
	0.15	bdl	1.62	*0.39*	0.89	0.03	0.26	*0.57*	0.02	bdl	0.07	*0.01*	0.02	bdl	0.08	*0.02*
NiO																
	0.02	bdl	0.07	*0.02*	0.01	bdl	0.02	*0.01*	0.02	bdl	0.07	*0.01*	0.01	bdl	0.06	*0.02*
ZnO																
	0.28	0.01	0.83	*0.24*	0.22	0.01	0.83	*0.35*	0.29	bdl	0.73	*0.02*	0.72	0.09	3.01	*0.62*
Na_2O																
	0.66	bdl	1.58	*0.47*	0.02	bdl	0.05	*0.02*	0.83	0.03	1.58	*0.38*	2.26	0.63	7.32	*1.49*
K_2O																
	94.1	85.4	100	*4.32*	98.2	96.2	100	*1.04*	93.3	85.4	100	*4.25*	93.3	2.5	98.8	*3.38*
Total																
Fe/Si (atomic)	0.86	0.03	2.52	*0.51*	0.61	0.13	0.86	*0.22*	0.93	0.03	2.52	*0.53*	0.25	0.03	0.67	*0.13*
Fe/Mg	35.7	2.7	186	*46.5*	0.67	0.28	0.97	*0.27*	43.3	6.8	186	*47.7*	10.3	1.37	56.1	*10.6*
Fe/Mn	804	38	4258	*1064*	78.5	38	110	*6.3*	1057	56	4258	*1126*	605	82	4242	*927*

Mg/Al	1.3	0.01	16.4	*3.52*	18.4	8.38	3 6.4	*1 0.7*	0.11	0.01	0.11	*0.03*	0.14	b dl	0.74	*0.16*
Mg/Si	0.19	0.01	1.23	*0.38*	1.06	0.88	1.23	*0.12*	0.1	0.01	0.1	*0.03*	0.04	b dl	0.16	*0.04*
Al_2O_3 +K_2O (w%)	15.2	1.23	33.1	*8.49*	2.53	1.23	3 6	*0.8*	33.1	2.13	33.1	*7.11*	22.2	9.4	40.4	*7.51*
K_2O+ Na_2O	0.94	0.01	2.1	*0.59*	0.24	0.01	0.88	*0.37*	1.12	2.17	2.1	*0.5*	2.87	0.96	7.41	*1.43*

n= number of spherules measured. Bdl : below detection limit.

Table 3

Distribution of textural group of the 161 extracted fossil CSs analyzed for triple oxygen isotopic composition,

and related percentage statistics for parent body origin.

Textural group	Number of analyzed spherules	%	OC related	%	CC related	%	Overlap with TFL (incl. CI, EC, HED)	%	Hydration zone (unidentified)	%
I-type	87	*54*	12	*100*	23	*34*	46	*62*	6	*75*
G/I-type	4	*2.5*	0	*0*	1	*1.5*	3	*4*	0	*0*
G-type	43	*28*	0	*0*	28	*41*	15	*20*	0	*0*
S-type	26	*17*	0	*0*	15	*22*	10	*14*	2	*25*
Total	160	*100*	12	*100*	67	*100*	74	*100*	8	*100*

Declaration of Interest Statement

☒ The authors declare that they have no known competing financial interests or personal relationships that could have appeared to influence the work reported in this paper.

☐ The author is an Editorial Board Member/Editor-in-Chief/Associate Editor/Guest Editor for this journal and was not involved in the editorial review or the decision to publish this article.

☐ The authors declare the following financial interests/personal relationships which may be considered as potential competing interests: